RESEARCH ARTICLE

Proposing several model techniques including ANN and M5P-tree to predict the compressive strength of geopolymer concretes incorporated with nano-silica

Hemn Unis Ahmed[1] · Ahmed S. Mohammed[1] · Azad A. Mohammed[1]

Abstract

Geopolymers are innovative cementitious materials that can completely replace traditional Portland cement composites and have a lower carbon footprint than Portland cement. Recent efforts have been made to incorporate various nanomaterials, most notably nano-silica (nS), into geopolymer concrete (GPC) to improve the composite's properties and performance. Compression strength (CS) is one of the essential properties of all types of concrete composites, including geopolymer concrete. As a result, creating a credible model for forecasting concrete CS is critical for saving time, energy, and money, as well as providing guidance for scheduling the construction process and removing formworks. This paper presents a large amount of mixed design data correlated to mechanical strength using empirical correlations and neural networks. Several models, including artificial neural network, M5P-tree, linear regression, nonlinear regression, and multi-logistic regression models, were utilized to create models for forecasting the CS of GPC incorporated with nS. In this case, about 207 tested CS values were collected from literature studies and then analyzed to promote the models. For the first time, eleven effective variables were employed as input model parameters during the modeling process, including the alkaline solution to binder ratio, binder content, fine and coarse aggregate content, NaOH and Na_2SiO_3 content, Na_2SiO_3/NaOH ratio, molarity, nS content, curing temperatures, and ages. The developed models were assessed using different statistical tools such as root mean squared error, mean absolute error, scatter index, objective function value, and coefficient of determination. Based on these statistical assessment tools, results revealed that the ANN model estimated the CS of GPC incorporated with nS more accurately than the other models. On the other hand, the alkaline solution to binder ratio, molarity, NaOH content, curing temperature, and ages were those parameters that have significant influences on the CS of GPC incorporated with nS.

Keywords Geopolymer concrete · Mix proportion · Nano-silica · Compressive strength · Modeling · Sensitivity

Introduction

The most frequently used construction material is concrete (Abdullah et al. 2021; Faraj et al. 2022). Yet, Portland cement is the primary cementing material used to bind the ingredients of the concrete composites (Sharif 2021). However, producing Portland cement necessitates a significant quantity of energy and raw materials, which creates a large amount of total carbon dioxide (about 7%) into the atmosphere (Mahasenan et al. 2003; Hamah Sor et al. 2021). However, cement-based concrete remains the most widely used material in the global building industry (Shaikh 2016). Therefore, it has become mandatory for all nations to consider CO_2 emission regulations and reductions (Yildirim et al. 2015). As a result, extensive research has been conducted to develop a new material that can be used as an alternative to Portland cement (Provis et al., 2015); among them, geopolymer technology was developed in France by Professor Davidovits (Abdel-Gawwad and Abo-El-Enein 2016). Due to the high consumption of waste materials in mixed proportions, GPC emits approximately 70% less green gas than conventional concrete (Weil et al. 2009).

✉ Hemn Unis Ahmed
hemn.ahmed@univsul.edu.iq; hemnunis@yahoo.com

1 Civil Engineering Department, College of Engineering, University of Sulaimani, Sulaimani, Kurdistan Region, Iraq

Geopolymers are an inorganic alumino-silicate polymer family produced through alkaline activation of various aluminosilicate virgin or waste materials rich in silicon and aluminum (Davidovits, 2015; Qaidi et al. 2022). The mixed proportions of the GPC consist of aluminosilicate source binder materials, fine and coarse aggregates, alkaline solutions, and water. The polymerization between the alkaline solutions and source binder materials produces solid concrete, almost like traditional concrete composites (Ahmed et al. 2021a). Many factors influenced the properties and performances of GPC, including the molarity of NaOH, the ratio of Na_2SiO_3/NaOH, curing regime and ages, water to solids ratio, alkaline solution to binder ratio, elemental composition and type of source binder materials, ratio of Si to Al in the geopolymer system, mixing time and rest period, superplasticizer dosage and extra water contents, and coarse and fine aggregate contents (Mohammed et al. 2021).

Nanotechnology is the ability to monitor and restructure matter at the atomic and molecular levels in the range of 1 to 100 nm, as well as the contribution to the distinct properties and phenomena at that size that are equivalent to those associated with individual atoms and molecules or bulk behavior (Roco et al. 2000). Nanotechnology is a burgeoning field of research, with novel science and practical applications gradually gaining prominence over the last two decades. Recently, efforts have been made to incorporate nanoparticles (NPs) into construction materials to improve the properties and performance of concrete (Lazaro et al. 2016). NPs were introduced with geopolymer matrices to enhance durability issues, physical structure, and mechanical properties of the geopolymer mixture (Assaedi et al. 2016). Because NPs have a higher surface area to volume ratio, they are highly reactive and have an effect on reaction rates (Wiesner and Bottero 2017). As a result, NPs modify the microstructure of GPC at the atomic level, resulting in significant improvements in both the fresh and hardened states, as well as microstructural behavior of geopolymer composites (Adak et al. 2017). In the literature, a wide range of NPs like nano-silica (nS) (Mustakim et al., 2020), nano-clay (nC) (Ravitheja and Kumar, 2019), nano-alumina (nA) (Shahrajabian and Behfarnia, 2018), carbon nanotubes (CNT) (Kotop et al. 2021), nano-metakaolin (Nm) (Rabiaa et al., 2020), and nano-titanium (nT) (Sastry et al. 2021) were consumed to improve various properties of the geopolymer composites, with nS being the most frequent as shown in Table 1. Since nano-silica was the most used nanomaterial to prepare geopolymer concrete composites (Ahmed et al. 2022) among all other NP types, therefore, this study was devoted to proposing different models to estimate the CS of GPC composites incorporated with nS.

Compression strength is a critical characteristic of all concrete composites, including GPC. The CS provides a broad assessment of the quality of the concrete (Ahmed et al.

2021b). However, the concrete's CS at 28 days is critical in structural design and construction. As a result, creating a credible model for estimating the CS of concrete is crucial in terms of modifying or validating the concrete mix proportions (Golafshani et al., 2020). Several factors influence the CS of GPC, resulting in a wide range of compression strength results; consequently, estimating CS is a problematic issue for scholars and engineers. As a result, new numerical and mathematical models are required to clarify this issue (Shahmansouri et al., 2020a). Machine learning methods have been utilized in the literature to model various features of concretes, such as the CS of green concrete (Velay-Lizancos et al., 2017), essential mechanical properties of recycled concrete aggregate (Gholampour et al., 2020), recycled concrete aggregate modulus of elasticity (Golafshani and Behnood, 2018), the CS of environmentally friendly GPC using natural zeolite and silica-fume (Shahmansouri et al., 2020b), the CS of nS-modified self-compacting concrete (Faraj et al., 2021), and the CS of fly ash-based GPC composites (Ahmed et al. 2021c).

In the literature, there is a shortage of studies examining the impact of different mixture proportion parameters on the CS of GPC incorporated with nS at various curing temperatures and ages. Also, according to a complete and systematic assessment of GPC, the construction industry rarely uses an authoritative and developed model that uses numerous parameters to estimate the CS of GPC incorporated with nS. Most efforts have focused on a single-scale model that does not account for a wide range of experimental data or factors. Moreover, the CS of GPC is influenced by several factors. As a result, in a single equation and model structure, the effects of eleven variables such as the alkaline solution to binder ratio (l/b), binder content (b), fine (FA) and coarse (CA) aggregate content, sodium hydroxide (SH) and sodium silicate (SS) content, the ratio of SS/SH, the molarity of SH (M), nS content, curing temperatures (T), and ages of concrete specimens (A) were considered and quantified on the CS of GPC incorporated with nS by using different model techniques, namely artificial neural network (ANN), M5P-tree (M5P), linear regression (LR), nonlinear regression (NLR), and multi-logistic (MLR) models. Finally, different statistical tools, such as the root mean squared error (RMSE), mean absolute error (MAE), scatter index (SI), OBJ value, and the coefficient of determination (R^2), were used to evaluate the created models' accuracy.

Research significance

The primary goal of this paper is to create multiscale models for estimating the CS of GPC incorporated with nS. Thus, a diverse range of laboratory work data, approximately 207 tested specimens with a variety of l/b, b, FA, CA, SH, SS,

Table 1 Properties and dosages of NPs reported in the literature to modify geopolymer concrete

References	Binder	Type of NPs	NPs%	Properties of NPs
Mustakim et al. 2020	F- GGBFS	nS	0, 0.5, 1, 1.5, 2, and 2.5%	NA
Çevik et al. 2018	F	nS	0.0 and 3%	99.8% SiO_2
Sastry et al. 2021	F	nT	0, 1, 2, 3, 4, and 5%	59.93% titanium and 40.55% oxygen, grain size (20–10 μm)
Rabiaa et al. 2020	GGBFS	nS	0, 2, 4, 6, and 8%	Particle size = 14 nm, surface area (m^2/g) = 200, 99.65% SiO_2
		nM	0, 2, 4, 6, and 8%	Particle size = 88.7 nm, surface area (m^2/g) = 140.792, 45.5% SiO2, 37% Al_2O_3
Adak et al. 2017	F	nS	0.0 and 6%	Particle size = 4–16 nm, solid content (%wt.) = 31, density (g/cm^3) = 2.37, viscosity (Pa·S) = 8.5, pH = 9.0–9.6
Behfarnia and Rostami 2017	GGBFS	nS	0, 0.5, 1, 3, and 5%	Purity (%) = 99.8, particle size = 20–30 nm, density (kg/m^3) = 200, Blain (m^2/g) = 193
Nuaklong et al. 2020	F+RHA	nS	0, 1, 2, and 3%	Purity (%) = 99.8, average size = 12 nm, surface area (m^2/g) = 200
Patel et al. 2015	F	nS	0, 0.5, 1, and 1.5%	Surface area (m^2/g) = 200 ± 25, average size = 12 nm, purity (%) = 99.8, pH in 4% dispersion = 3.4–4.7, moisture 2 h at 105 °C (wt.%) ≤ 1.5
Ibrahim et al 2018a	NP	nS	0, 1, 2.5, 5, and 7.5%	Solid content (%) = 50, average particle size (nm) = 35, bulk density (g/cm^3) = 1.4, specific surface area (m^2/g) = 80, Na_2O content (%) = 0.2, viscosity (cps) = 15, pH = 9.5
Mahboubi et al. 2019	MK	nS	0, 1, 2, and 3%	NA
		nC	0, 1, 2, and 3%	
Naskar and Chakraborty 2016	F	nS	0, 0.75, 3, and 6%	NA
		nT	0.0 and 1%	
		CNT	0.0 and 0.02%	
Nuaklong et al. 2018	F+OPC	nS	0, 1, 2, and 3%	Average diameter = 40 nm, density = 0.13 g/cm^3, BET specific area = 50 m^2/g, purity (%) = 99.8
Ravitheja and Kumar 2019	F+GGBFS	nC	0, 4, 6, 8, and 10%	NA
Emad et al. 2018	GGBFS	nS	0.0 and 2%	Average particle size = 30 nm, surface area = 45 m^2/g, purity (%) = 99.17
Vyas et al. 2020	F	nS	0, 2, 4, 6, and 8%	Average particle size = 10 nm
Etemadi et al. 2020	GGBFS	nS	0, 1, 2, and 3%	NA
Angelin Lincy and Velkennedy 2020	GGBFS	nS	0, 0.5, and 1%	Purity (%) = 99.9, surface area (m^2/g) = 201, specific gravity = 2.34
Saini and Vattipalli 2020	GGBFS	nS	0.0 and 2%	Purity (%) = 99.88, particle Size = 17 nm, specific gravity = 2.3, specific surface area (m^2/g) = 202, pH value = 4.12, tamped density (g/L) = 44
Kotop et al. 2021	F+GGBFS	nC	0, 2.5, 5, and 7%	SiO_2 = 61.24, Al_2O_3 = 20.89
		CNT	0.01, 0.02%	Length = 10–100 mm, inner diameter = 1.5–15 nm, outer diameter = 50 nm
Ibrahim et al 2018b	NP	nS	0, 1, 2.5, 5, and 7.5%	Solid content (%) = 50, average particle size (nm) = 35, bulk density (g/cm^3) = 1.4, specific surface area (m^2/g) = 80, Na_2O content (%) = 0.2, viscosity (cps) = 15, pH = 9.5
Shahrajabian and Behfarnia 2018	GGBFS	nA	0, 1, 2, and 3%	Particle size (nm) = 20, Blaine (m^2/g) = 100, purity (%) = 99.7
		nC	0, 1, 2, and 3%	Particle size (nm) = 1–2, Blaine (m^2/g) = 220–270, density (g/cm^3) = 0.5–0.7
		nS	0, 1, 2, and 3%	Particle size (nm) = 11–13, Blaine (m^2/g) = 200, density (g/cm^3) = 2.4, purity (%) = 99
Their and Özakça, 2018	F- GGBFS	nS	0.0 and 2%	Specific surface area = 170–230 m^2/g, specific gravity = 2.2, purity (%) = 99.8

Table 1 (continued)

References	Binder	Type of NPs	NPs%	Properties of NPs
Ibrahim et al. 2018c	NP	nS	0, 1, 2.5, 5, and 7.5%	Solid content (%) = 50, average particle size (nm) = 35, bulk density (g/cm³) = 1.4, specific surface area (m²/g) = 80, Na₂O content (%) = 0.2, viscosity (cps) = 15, pH = 9.5
Janaki et al. 2021	GGBFS + SF	CNT	0, 2,5, and 10%	CNTs have diameter of 20 to 120 nm and are several micrometers in length

NPs, nano-particles; *F*, fly ash; *GGBFS*, ground granulated blast furnace slag; *MK*, metakaolin; SF, silica fume; *RHA*, rice husk ash; *NP*, natural pozzolan; *OPC*, ordinary Portland cement; *nS*, nano-SiO2; *nT*, nano-TiO2; *nM*, nano-metakaolin; *nC*, nano-clay; *CNT*, carbon nanotube; *nA*, nano-Al2O3

M, SS/SH, nS, T, and ana A, were collected and reviewed using a variety of analytical approaches with the goal of (i) providing most effortless equations to be used by practicing engineers and scholars in their GPC mix design works; (ii) clarifying the effects of each mix proportion parameter and curing temperature and age on the CS of GPC incorporated with nS; (iii) quantifying and offering systematic multiscale models for forecasting the CS of GPC utilizing eleven variable input parameters; (iv) using statistical assessment methods such as MAE, RMSE, R^2, OBJ, and SI to find the most authoritative model to forecast the CS of GPC composites incorporated with nS from various model strategies (LR, NLR, MLR, ANN, and M5P).

Methodology

The authors conducted an extensive search of several databases, including Research Gate, Science Direct, Google Scholar, Scopus, and the Web of Science. A wealth of papers was discovered discussing the effect of various NP types on the properties of geopolymer paste composites. However, a limited number of documents were found regarding the impact of NPs on the properties of GPC composites. In total, 207 datasets of the CS values were obtained. In the literature, a wide range of NPs like nS, nC, nA, CNT, nM, and nT were consumed to improve various properties of the GPC composites, with nS being the most frequent, as can be seen in Table 1. Therefore, in this study, the authors take those articles that used nS to improve various properties of the GPC composites.

In the modeling process, eleven input parameters were used, limiting the authors' ability to utilize a greater number of data in the created models. The gathered datasets were statistically analyzed and classified into three groups. The models were built using the larger group, which included 135 datasets. The second group is made up of 36 datasets that were used to test the created models, and the final group is made up of 36 datasets that were

consumed to validate the suggested models (Golafshani et al. 2020; Faraj et al. 2021). Table 2 shows the dataset ranges, including all significant parameters and the observed CS of the GPC incorporated with nS. The input dataset contains the following values: *l/b* ranges from 0.4 to 0.4, *b* ranges from 300 to 500 kg/m³, FA ranges from 490 to 990 kg/m³, CA ranges from 810 to 1470 kg/m³, SH ranges from 18.17 to 159.75 kg/m³, SS ranges from 40.8 to 187.5 kg/m³, *M* ranges from 4 to 16 M, SS/SH ranges from 0.33 to 3, nS ranges from 0 to 60 kg/m³, *T* ranges from 23 to 70 °C, *A* ranges from 0.5 to 180 days, and CS ranges from 3.2 to 81.3 MPa. The previous datasets were used to propose various models such as LR, NLR, MLR, ANN, and M5P to estimate the CS of GPC incorporated with nS; then, the developed models were evaluated using statistical criteria such as R^2, RMSE, MAE, SI, and OBJ to determine the most reliable and accurate model. Additional details about this work's methodology are shortened in a flowchart, as illustrated in Fig. 1.

Statistical assessment

Sufficient information about each variable input model parameter is provided in the following sections through "Alkaline solution to binder ratio (*l/b*)" to "Compressive strength (CS)."

Alkaline solution to binder ratio (l/b)

Based on the collected datasets, the ratio of *l/b* of the GPC mixtures modified with nS was in the range of 0.4 to 0.6, with the average and standard deviations of 0.49 and 0.05, respectively. Also, regarding other statistical analyses, it was found that the variance was 0.002, skewness was 0.66, and the kurtosis was −0.25. Figure 2 depicts the relationship between CS and *l/b* with histograms of GPC mixtures incorporated with nS.

Table 2 Summary of the constitutes of geopolymer concrete mixes reported in the literature

Ref	l/b	b (kg/m³)	FA (kg/m³)	CA (kg/m³)	SH (kg/m³)	SS (kg/m³)	M	SS/SH	nS (kg/m³)	T (°C)	A (days)	CS (MPa)
Mustakim et al. 2020	0.45	486–490	490	1470	73	154	12	2	0–3.675	31.5	3_28	8.95–62.8
Çevik et al. 2018	0.45	500	575	1150	64.3	160.7	14	2.5	0–15	70	30	51.63–42.71
Rabiaa et al. 2020	0.45	500–460	790	907	62.5	187.5	12	2.33	0–40	28	7_28	29–48
Adak et al. 2017	0.4	440	723	1085	64	112	12	1.75	0–26.4	28–60	3_28	21.7–46.43
Behfarnia and Rostami 2017	0.45	393–414	692–684	1240–1233	46.6–44.2	139.7–132.6	4	3	0–20.7	23	28–60	52–76.5
Nuaklong et al. 2020	0.6	450	500	970–1150	135	135	10	1	0–13.5	25	7_90	18.6–47.3
Patel et al. 2015	0.45	380.689	554.4	1295	48.945	122.364	8_16	2.5	0–5.71	60	28	38.1
Ibrahim et al 2018a	0.52	370–400	650	1206	60	150	14	2.5	0–30	60	1_28	4.7–45
Mahboubi et al. 2019	0.6	300	800	1200	85	95	12	1.1	0–9	25	7_28	18.9–45.9
Naskar and Chakraborty 2016	0.5	339–350	720	1305	43.5–45	108.9–112.5	16	2.5	0–21	60	7_28	3.2–24.4
Nuaklong et al. 2018	0.6	450	500	1036–1150	108	162	12	1.5	0–9	60	28	31.6–42.6
Vyas et al. 2020	0.45	497	560	1120	159.75	63.9	12	0.4	0–49.7	60	28	24–35
Etemadi et al. 2020	0.5	450	750	1000	75	150	12	2	0–13.5	25	7_28	21.9–50.4
Angelin Lincy and Velkennedy, 2020	0.4	394.29	554.4	1293.6	45.06	112.64	12	2.5	0–3.94	24	28	44.3–48.6
Saini and Vattipalli 2020	0.45	450–500	825	825	18.17–28.57	144.65–160.75	10_16	2.5	0–10	60	7_90	41.1–81.3
Ibrahim et al 2018b	0.52	370–400	620–650	1152–1206	60	150	14	2.5	0–60	24	3–180	4.3–61.2
Shahrajabian and Behfarnia 2018	0.45	362.8	990	810	122.4	40.8	4	0.33	0–10.88	25	7–120	35.5–61.8
Their and Özakça, 2018	0.45	405.8–413.8	888	945	53.2	133	12	2.5	0–8.3	29	28–90	37.1–52.3
Ibrahim et al. 2018c	0.52	370–400	620–650	1152–1206	60	150	14	2.5	0–60	60	0.5–28	4.9–45.1
Min	0.4	300	490	810	18.17	40.8	4	0.33	0	23	0.5	3.2
Max	0.6	500	990	1470	159.75	187.5	16	3	60	70	180	81.3
St.Dev	0.1	51.9	135.3	183.3	33.9	35.6	3.3	0.8	14.6	17.4	31.8	17.5

l/b, alkaline solution to binder ratio; *b*, binder content (kg/m³); *FA*, fine aggregate content (kg/m³); *CA*, coarse aggregate content (kg/m³); *SH*, sodium hydroxide content (kg/m³); *SS*, sodium silicate content (kg/m³); *M*, molarity (M); *SS/SH*, ratio of sodium silicate to sodium hydroxide; *nS*, nano-silica content (kg/m³); *T*, curing temperature (°C); *A*, age (days); and *CS*, tested compressive strength (MPa)
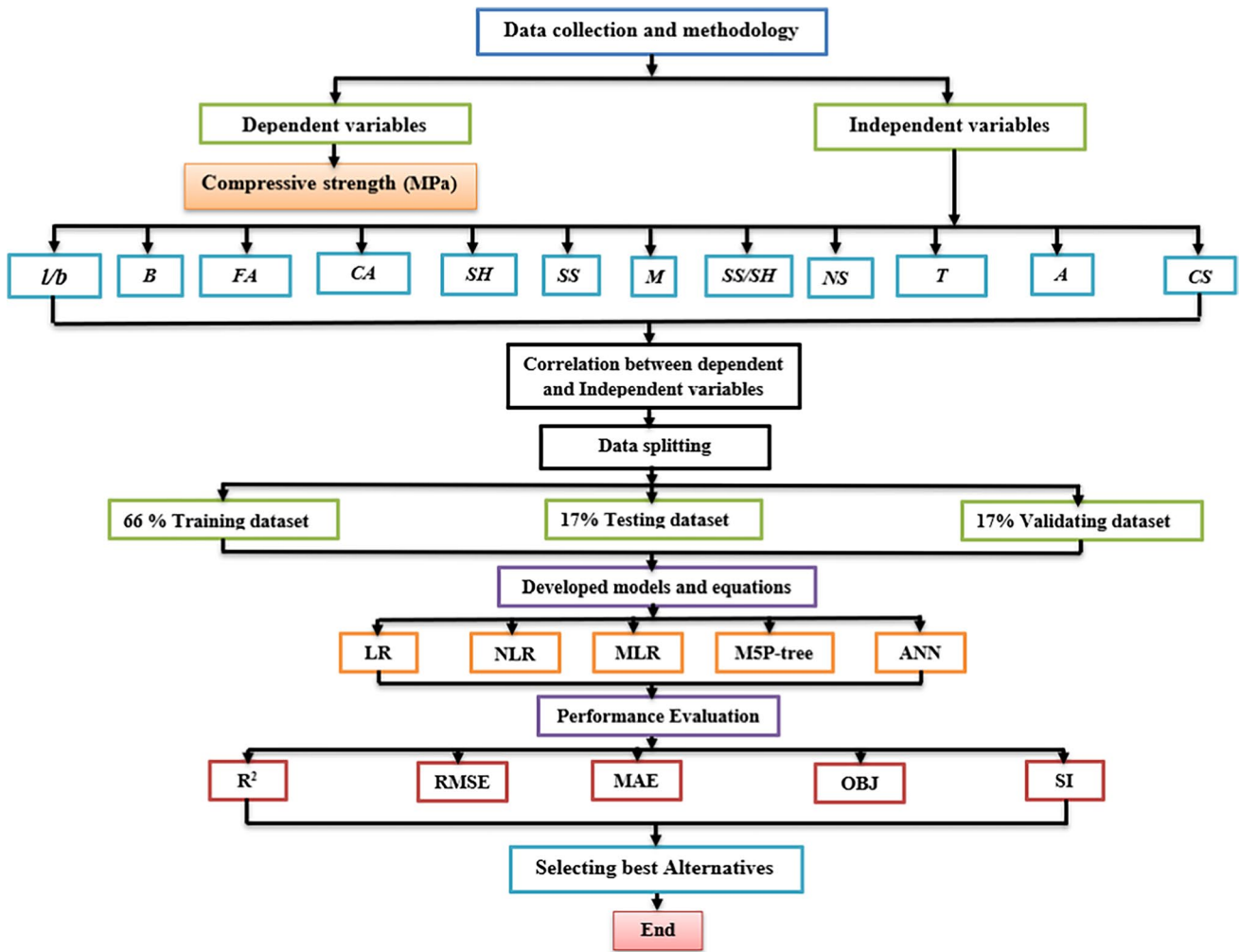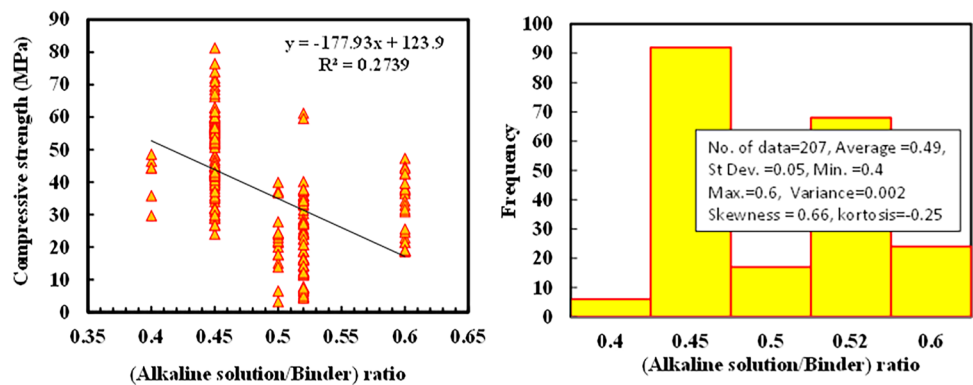
Fig. 1 The flowchart diagram process followed in this study

Fig. 2 Correlations between CS and *l/b* ratio with histogram of GPC mixtures incorporated with nS


Binder content (b)

According to Table 1, F, GGBFS, MK, SF, RHA, and NP are those ashes that scholars used as source binder materials to produce GPC composites. The ranges of these binders were between 300 and 500 kg/m^3, with the average and standard deviations of 417 kg/m^3 and 51.8 kg/m^3, correspondingly. At the same time, other statistical assessment tools like variance, skewness, and kurtosis were 2689, 0.11, and − 0.81, respectively, for the collected datasets. Figure 3 illustrates the CS and *b* content variation and frequencies of the gathered data of GPC mixtures incorporated with nS.

Fig. 3 Correlations between CS and binder content with histogram of GPC mixtures incorporated with nS
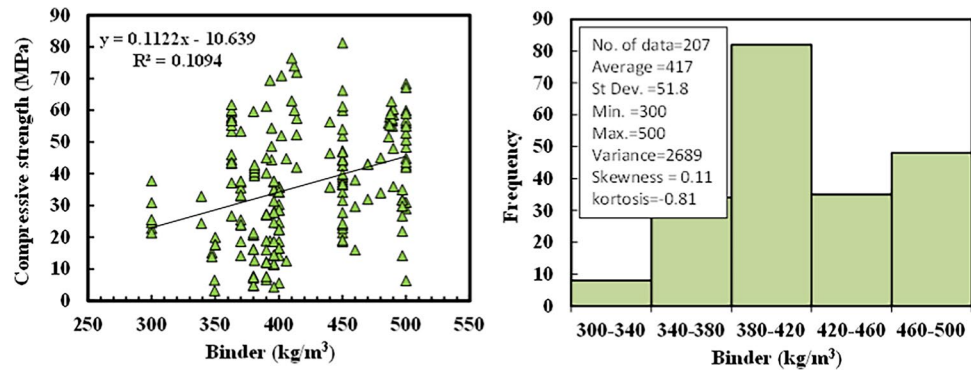
Fine aggregate content (FA)

Like traditional concrete mixtures, natural and crushed sands were used as the FA in GPC mixtures. The FA should be satisfied with the requirements of ASTM standards. According to gathered datasets from the literature article, it was found that the range of FA was between 490 and 990 kg/m^3, with an average of 681 kg/m^3 and standard deviations of 135.2 kg/m^3. More information regarding other statistical assessment tools can be found in Fig. 4.

Coarse aggregate content (CA)

Natural, crushed, and recycled aggregates are those forms of aggregates that were used as the CA in geopolymer concrete mixtures, just like conventional concrete mixtures. Same as FA, the CA should have all the properties which are required by ASTM standards. Regarding the ranges of CA, it was concluded that the contents of CA in past research varied between 810 and 1470 kg/m^3 with an average of 1113.8 kg/m^3 and standard deviations of 183.2 kg/m^3. On the other hand, the variance, skewness, and kurtosis were 33,580, -0.19, and -0.71, respectively. Also, the correlations between the CS of tested datasets and the CA contents can be found in Fig. 5.

NaOH content (SH)

Pellets and flakes are two forms of SH in a solid state with a purity above 97%. This material is mixed with the required amount of water to prepare a solution of SH with the required molarity. In this study, according to the collected datasets, the amount of SH in 1 m^3 of GPC mixtures incorporated with nS was in the range between 18.1 and 159.7 kg/m^3, with an average of 71.3 kg/m^3 and a standard deviation of 33.9 kg/m^3. Extra information about other statistical assessment criteria and correlations between the CS and SH content can be found in Fig. 6.

Na$_2$SiO$_3$ content (SS)

Water glass or sodium silicate is present in a liquid form which mainly consists of Na$_2$O, SiO$_2$, and H$_2$O. Based on the previous research conducted on the GPC mixtures incorporated with nS, the range of SS was found between 40.8 and 187.5 kg/m^3, with an average of 134.4 kg/m^3 and the standard deviations of 35.6 kg/m^3. In comparison, other stats information like variance, skewness, and kurtosis were 1268, -1.42, and 1.55, correspondingly. Furthermore, the correlations between the CS and the SS contents of GPC can be found in Fig. 7.

Fig. 4 Correlations between CS and FA content with histogram of GPC mixtures incorporated with nS
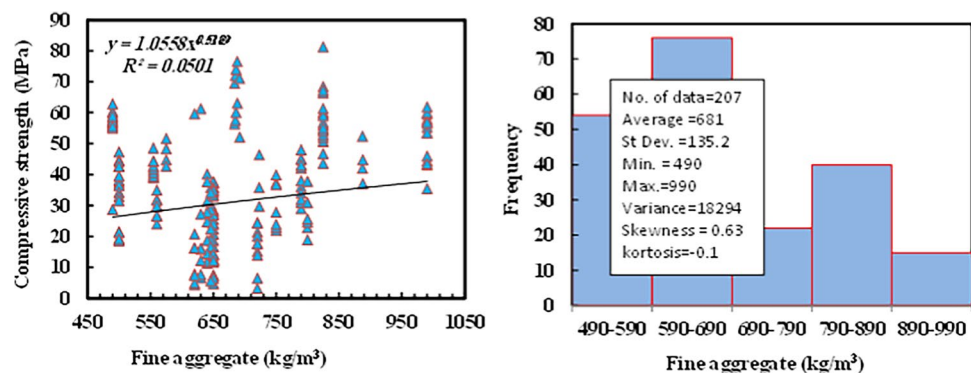
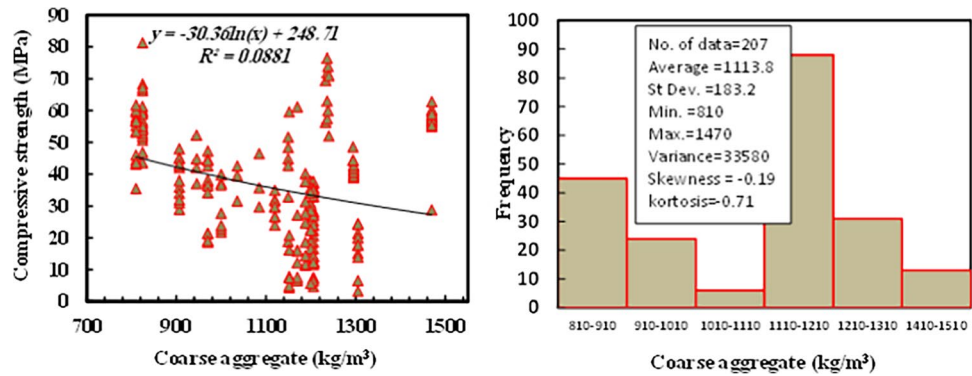**Fig. 5** Correlations between CS and CA content with histogram of GPC mixtures incorporated with nS

Fig. 6 Correlations between CS and SH content with histogram of GPC mixtures incorporated with nS
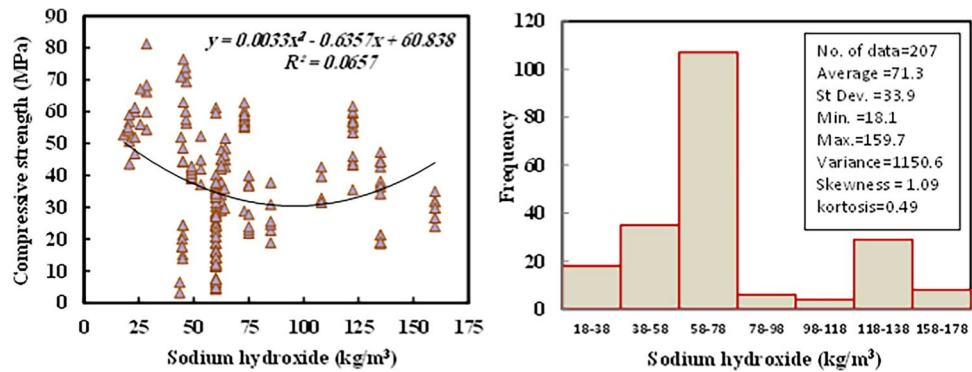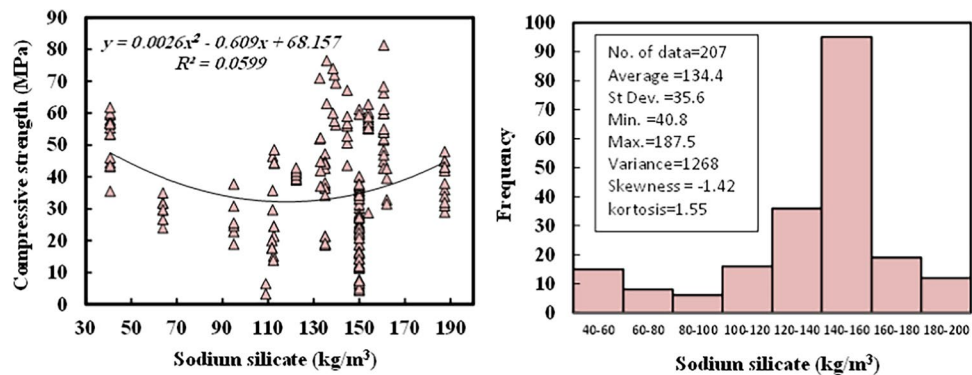

**Fig. 7** Correlations between CS and SS content with histogram of GPC mixtures incorporated with nS

Molarity (M)

In the field of GPC science, the concentrations of sodium hydroxide inside water were called molarity. The authors of this study found that the molarity of SH in the collected papers was in the range between 4 and 16 M, with an average of 11.9 M and standard deviations of 3.3 M. Also, it was found that the variance of the reviewed datasets was 11.1, the skewness was -1.4, and kurtosis was 1.3. The variations between the CS and M with the frequency of their datasets of GPC incorporated with nS are presented in Fig. 8.

Na$_2$SiO$_3$/NaOH (SS/SH)

This parameter consists of a mixture of SS and SH with the required molarity. Usually, it is prepared about 24 h before mixing the GPC ingredients. According to the gathered datasets, this parameter was used in the range between 0.33 and 3, with an average of 2.05 and standard deviations of 0.76. Also, the other statistical criteria were found to be 0.59, -1.2, and 0.22 for the variance, skewness, and kurtosis, respectively. Moreover, correlations between the CS and the SS/SH are illustrated in Fig. 9, with the frequencies of their datasets.

Fig. 8 Correlations between CS and molarity of SH with histogram of GPC mixtures incorporated with nS
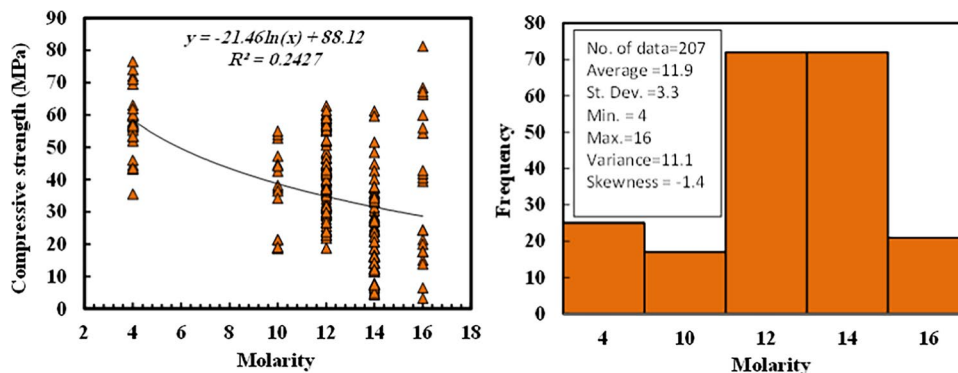
Nano-silica (nS) content

As mentioned earlier, nS was the most frequently NPs that scholars used to improve various properties of GPC composites. It was used as a binder replacement or just by the addition. Table 1 shows the different properties of nS and other NP types that were utilized in GPC composites. Regarding the values of this input model parameter, it was found that the range of nS was used to improve GPC composites in the range between 0 and 60 kg/m³, with an average of 11.6 kg/m³, and the standard deviation of 14.5 kg/m³. Similarly, other statistical criteria with the correlations between the CS and the nS content can be found in Fig. 10.

Curing temperatures (T)

Ambient, steam, and oven curing regimes were commonly used to cure GPC composites. One of the reasons behind using NPs in GPC composites is to take away from the oven and steam curing methods and go toward ambient curing methods. Based on the collected datasets, GPC specimens modified with nS were cured in the temperature ranges between 23 and 70 °C, with an average of 42.05 °C and the standard deviations of 17.4 °C. Also, other statistical assessment tolls like variance, skewness, and kurtosis were 303.9, 0.11, and − 1.92, respectively. The variations of the CS with the nS content and the frequencies of nS datasets are presented in Fig. 11.

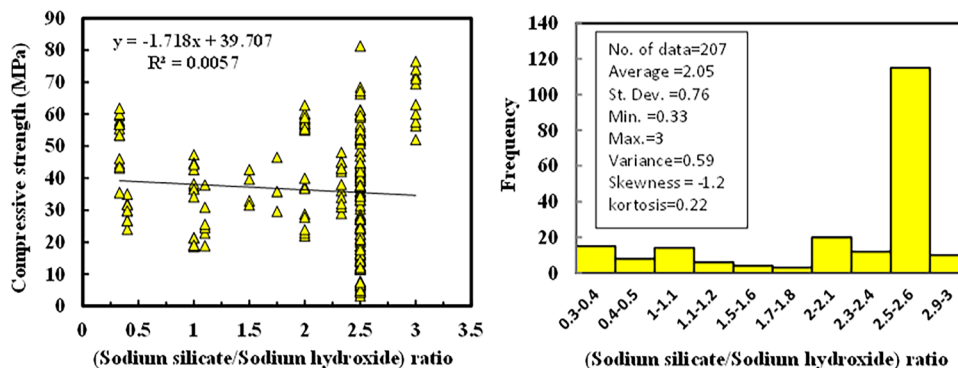**Fig. 9** Correlations between CS and SS/SH ratio with histogram of GPC mixtures incorporated with nS

Fig. 10 Correlations between CS and nS content with histogram of GPC mixtures incorporated with nS
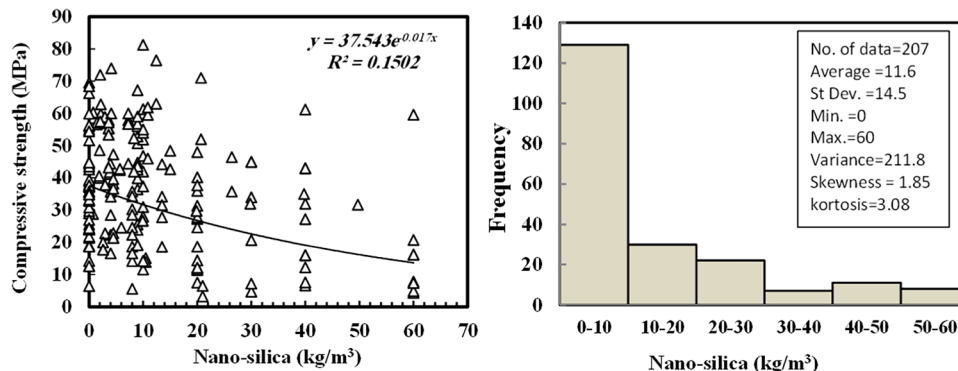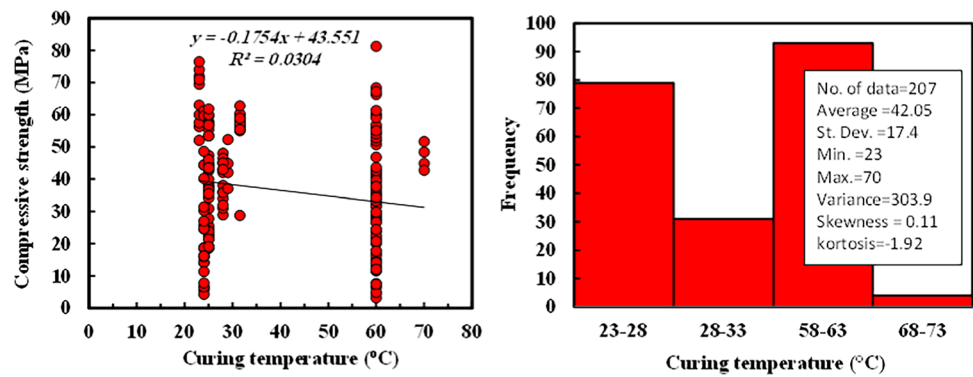
Fig. 11 Correlations between CS and T with histogram of GPC mixtures incorporated with nS

Age of specimens (A)

To gain sufficient early and late CS, the curing ages should be extended to promote the polymerization process, which strengthens geopolymers. Thus, based on the collected datasets, the cure time for GPC incorporated with nS ranged from 0.5 to 180 days, with an average of 28 days and standard deviations of 31.8 days. Similarly, the published datasets' variance, skewness, and kurtosis were 1012.8, 2.36, and 6.96, respectively. The relationships between the CS and the specimen ages with the frequencies of collected data are shown in Fig. 12.

Compressive strength (CS)

An applied vertical load per unit area of the GPC specimens was known as normal stress or compressive strength. This property is one of the critical mechanical properties of GPC composites. As shown in Table 2, the range of the CS for the gathered datasets was in the range between 3.2 and 81.3 MPa, with an average of 36.2 MPa and standard deviations of 17.52 MPa. At the same time, other statistical criteria like variance, skewness, and kurtosis were 307, 0.15, and − 0.75, respectively.

Modeling

Based on the coefficients of the determinations (R^2) of the collected input model parameters, as shown in Figs. 2, 3, 4, 5, 6, 7, 8, 9, 10, 11, and 12, there is no direct relationship between the CS and any individual input model parameters. Therefore, multiscale model techniques, including M5P, MLR, ANN, LR, and NLR, are employed to develop empirical models to forecast the CS of GPC composites incorporated with nS in different mix proportion parameters, curing regimes, and specimen ages.

For creating the models, the collected datasets are split into three categories. The models were built using the larger group, which included 135 datasets. The second group is made up of 36 datasets that were utilized to test the created models, and the final group is made up of 36 datasets that were consumed to validate the suggested models (Golafshani et al. 2020; Faraj et al. 2021). The forecasts of various models were compared employing these criteria: (1) The model's validity should be established scientifically; (2) between estimated and tested data, it should have a lower percentage of error; (3) the RMSE, OBJ, and SI values of the suggested equations should be low, while the R^2 value should be high.

Fig. 12 Correlations between CS and A with histogram of GPC mixtures incorporated with nS
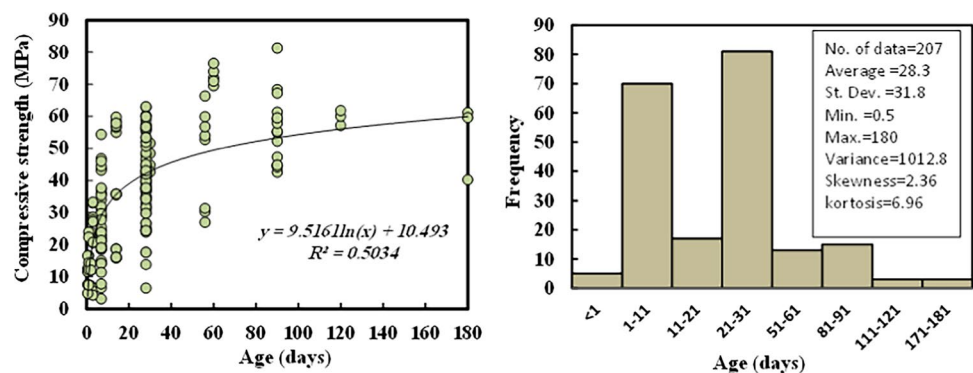
(a) **Linear regression model (LR)**

LR is one of the standard methods that scholars used to estimate and forecast the CS of concrete composites (Faraj et al., 2021). This model has a general form, as depicted in Eq. (1) (Ahmed et al. 2021c).

$$CS = a + b(x1) \tag{1}$$

where, CS, $x1$, a, and b represent the compressive strength, one of the variable input parameters, and model parameters, respectively. This equation contains just one variable of input data, so to have more practical and reliable investigations, Eq. (2) is suggested, which contains a wide range of input variable data parameters that can cover all of the geopolymer concrete mixture proportions and curing conditions, as well as curing ages.

$$CS = a + b\left(\frac{l}{b}\right) + c(b) + d(FA) + e(CA) + f(SH) \\ + g(SS) + h(M) + i\left(\frac{SS}{SH}\right) + j(nS) + k(T) + l(A) \tag{2}$$

As mentioned earlier, all these main variables in Eq. (2) were described except that the a, b, c, d, e, f, g, h, i, j, k, and l are the model parameters. Equation (2) is a one-of-a-kind equation because it incorporates a large number of independent variables to generate GPC incorporated with nS that may be extremely useful in the construction industry. On the other hand, because all variables can be adjusted linearly, the proposed Eq. (2) can be considered an extension of Eq. (1).

(b) **Nonlinear regression model (NLR)**

In terms of the NLR, Eq. (3) may be regarded as a general form for proposing an NLR model (Ahmed et al. 2021c).

The interrelationships between the variables in Eqs. (1) and (2) can be used to calculate the CS of normal geopolymer concrete mixtures and geopolymer concrete mixtures modified with nS using Eq. (3).

$$CS = a * \left(\frac{l}{b}\right)^b * (b)^c * (FA)^d * (CA)^e * (SH)^f * (SS)^g \\ * (M)^h * \left(\frac{SS}{SH}\right)^i * (T)^j * (A)^k + l \\ * \left(\frac{l}{b}\right)^m * (b)^n * (FA)^o * (CA)^p * (SH)^q * (SS)^r \\ * (M)^s * \left(\frac{SS}{SH}\right)^t * (T)^u * (A)^v * (nS)^w \tag{3}$$

where: all of the variables in this equation were provided earlier, except that the a, b, c, d, e, f, g, h, i, j, k, l, m, n, o, p, q, r, s, t, u, and v are described as a model parameter.

(iii) **Multi-logistic regression model (MLR)**

As with the previous models, the collected datasets were subjected to multi-logistic regression analysis, and the general form of the MLR is shown in Eq. (4) based on the research conducted by Ahmed et al. (2021c) and Faraj et al. (2021). MLR is used to distinguish a nominal predictor variable from one or more independent variables.

$$CS = a * \left(\frac{l}{b}\right)^b * (b)^c * (FA)^d * (CA)^e * (SH)^f * (SS)^g \\ * (M)^h * \left(\frac{SS}{SH}\right)^i * (nS)^j * (T)^k * (A)^l \tag{4}$$

where: all of the variables in this equation were provided earlier. Moreover, in this equation, the value of nS should be greater than 0.

(iv) **Artificial neural network (ANN)**

ANN is a powerful simulation software designed for data analysis and computation that processes and analyzes

Table 3 The tested ANN architectures	No. of hidden layers	No. of neurons in left side	No. of neurons in right side	R^2	MAE (MPa)	RMSE (MPa)
	1	1	0	0.9114	5.8711	7.545
	1	2	0	0.9346	5.0137	6.1308
	1	9	0	0.9744	2.631	3.849
	1	11	0	0.9707	2.9734	4.1676
	2	1	1	0.9085	6.144	7.8757
	2	3	3	0.9495	4.2999	5.4882
	2	5	5	0.9707	3.1309	4.2717
	2	7	7	0.9731	2.8988	4.0177
	2	9	9	0.9741	3.1746	4.297
	2	11	11	0.9768	2.8848	4.0084
	2	**12**	**12**	**0.9771**	**2.8316**	**3.892**
	2	13	13	0.9761	2.8787	3.9387
	2	17	17	0.9752	3.0827	4.1476

Fig. 13 Comparison between tested and predicted CS of GPC mixtures incorporated with nS using LR model: **a** training data, **b** testing data, **c** validating data
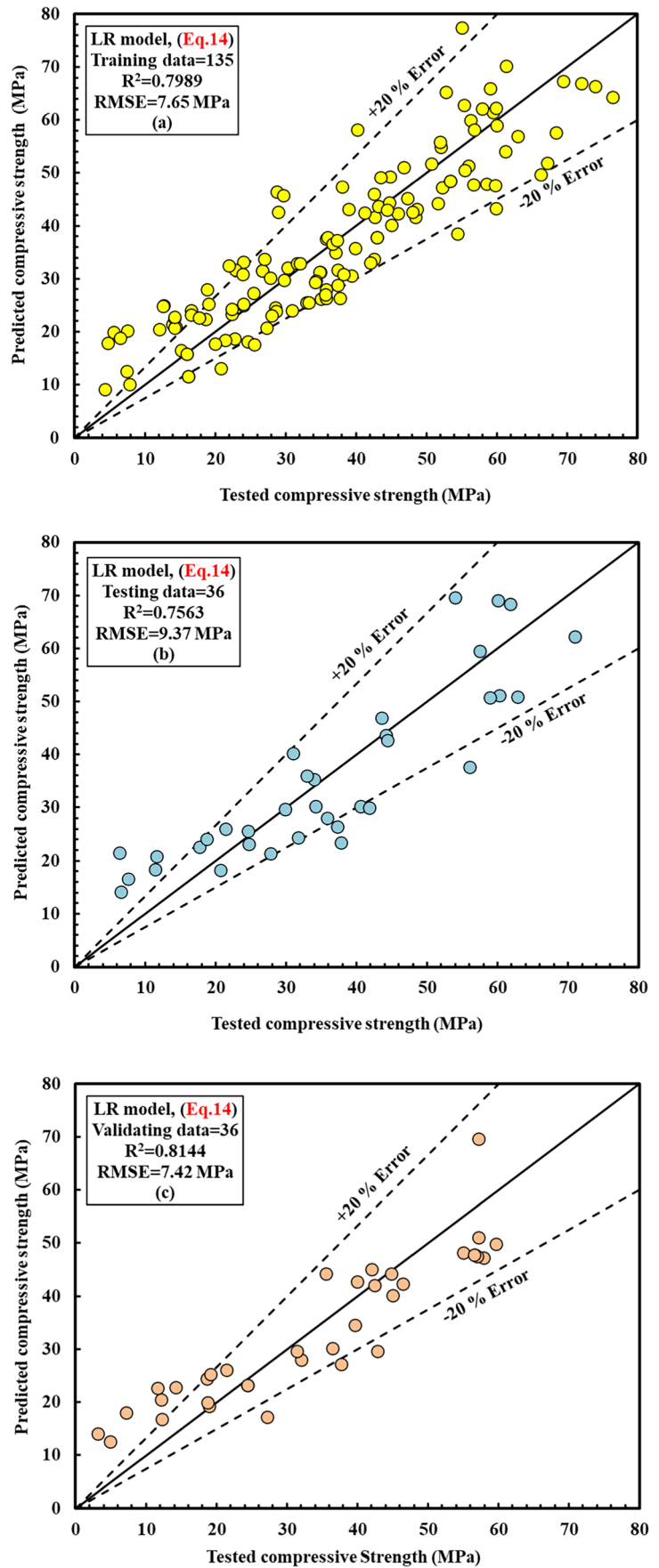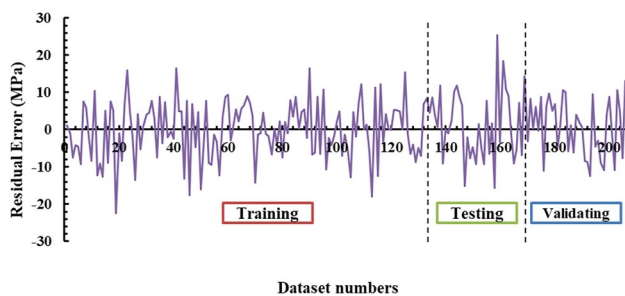
Fig. 14 Residual error diagram of CS of GPC mixtures incorporated with nS using training, testing, and validating datasets for LR model

data similarly to a human brain. This machine learning tool is widely used in construction engineering to forecast the future behavior of a variety of numerical problems (Mohammed 2018; Sihag et al. 2018).

An ANN model is generally divided into three main layers: input, hidden, and output. Depending on the proposed problem, each input and output layer can be one or more layers. On the other hand, the hidden layer is usually ranged for two or more layers. Although the input and output layers are generally determined by the collected data and the purpose of the designed model, the hidden layer is determined by the rated weight, transfer function, and bias of each layer to other layers. A multi-layer feed-forward network is constructed using a combination of proportions, weight/bias, and several parameters as inputs, including (l/b, b, FA, CA, etc.), and the output ANN is compressive strength.

There is no standardized method for designing network architecture. As a result, the number of hidden layers and neurons is determined through a trial and error procedure. One of the primary goals of the network's training process is to determine the optimal number of iterations (epochs) that provide the lowest MAE, RMSE, and best R^2-value close to 1. The effect of several epochs on lowering the MAE and RMSE has been studied. For the purpose of training the designed ANN, the collected dataset (a total of 207 data) was divided into three parts. Approximately 70% of the collected data was used as training data to train the network. The dataset was tested with 15% of the total data, and the remaining data were used to validate the trained network (Demircan et al., 2011). The designed ANN was trained and tested for various hidden layers to determine the optimal network structure based on the fitness of the predicted CS of GPC incorporated with nS with the CS of the actual collected data. It was observed that the ANN structure with two hidden layers, 24 neurons, and a hyperbolic tangent transfer function was a best-trained network that provides a maximum R^2 and minimum both MAE and RMSE (shown in Table 3). As a part of this work, an ANN model has been used to estimate the future value of the CS

of GPC incorporated with nS. The general equation of the ANN model is shown in Eqs. (5), (6), and (7).

From linear node 0:

$$CS = Threshold + \left(\frac{Node1}{1 + e^{-B1}}\right) + \left(\frac{Node2}{1 + e^{-B2}}\right) + \ldots \quad (5)$$

From sigmoid node 1:

$$B1 = Threshold + \sum (Attribute * Variable) \quad (6)$$

From sigmoid node 2:

$$B2 = Threshold + \sum (Attribute * Variable) \quad (7)$$

(e) **M5P-tree model (M5P)**

The M5P model tree reconstructs Quinlan's M5P-tree algorithm (Quinlan 1992), a decision tree with a linear regression function added to the leaf nodes. The decision tree encapsulates the algorithms in a tree structure formed by nodes formed during training on data. The nodes of the decision tree are classified as root nodes, internal nodes, and leaf nodes. Nodes are interconnected through branches until the leaves are reached (Malerba et al., 2004). Mohammed (2018) also introduced the M5P-tree as a robust decision tree learner model for regression analysis. The linear regression functions are placed at the terminal nodes by this learner algorithm. Classifying all datasets into multiple sub-spaces assigns a multivariate linear regression model to each sub-space. The M5P-tree algorithm operates on continuous class problems rather than discrete segments and is capable of handling tasks with a high number of dimensions. It reveals the developed information of each linear model component constructed to estimate the nonlinear correlation of the datasets. The information about division criteria for the M5-tree model is obtained through the error calculation at each node. The standard deviation of the class entering that node at each node is used to analyze errors. At each node, the attribute that maximizes the reduction of estimated error is used to evaluate any task performed by that node. As a result of this division in the M5P tree, a large tree-like structure will be generated, which will result in overfitting. The enormous tree is trimmed in the followed step, and linear regression functions restore the pruned subtrees. The general equation form of the M5P-tree model is the same as the linear regression equation, as shown in Eq. (8).

$$CS = a + b\left(\frac{l}{b}\right) + c(b) + d(FA) + e(CA)$$
$$+ f(SH) + g(SS) + h(M) + i\left(\frac{SS}{SH}\right) + j(nS) + k(T) \quad (8)$$
$$+ l(A)$$

where: the descriptions of all of the variables in this Eq. (8) were provided earlier.

Fig. 15 Comparison between tested and predicted CS of GPC mixtures incorporated with nS using NLR model: **a** training data, **b** testing data, **c** validating data
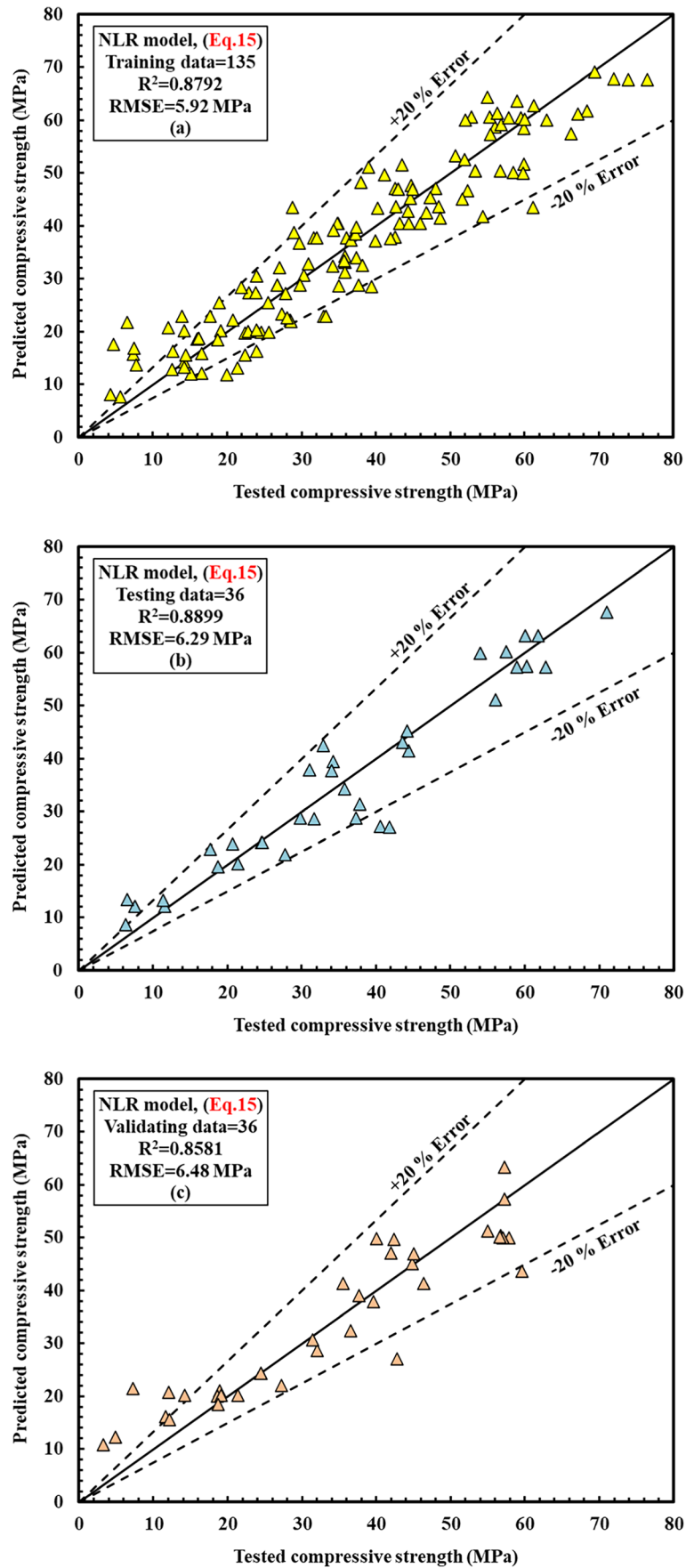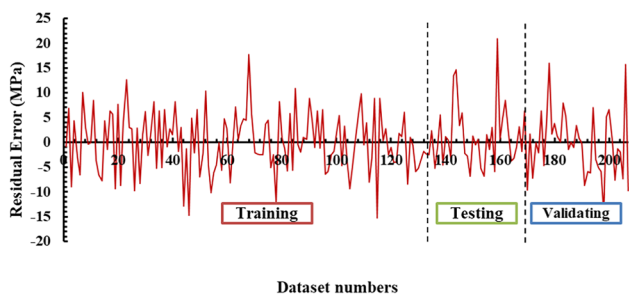
Fig. 16 Residual error diagram of CS of GPC mixtures incorporated with nS using training, testing, and validating datasets for NLR model

Model efficiencies

To rate and assess the proposed models' accuracy, various performance stats tools such as R^2, RMSE, MAE, SI, and OBJ were used, which they have the following equations:

$$R^2 = \left(\frac{\sum_{p=1}^{p} \left(y_p - y\right)\left(x_p - x'\right)}{\sqrt{\left[\sum_{p=1}^{p} \left(y_p - y'\right)^2\right]\left[\sum_{p=1}^{p} \left(x_p - x'\right)^2\right]}} \right)^2 \quad (9)$$

$$RMSE = \sqrt{\frac{\sum_{p=1}^{p} \left(x_p - y_p\right)^2}{n}} \quad (10)$$

$$MAE = \frac{\sum_{p=1}^{p} |(x_p - y_p)|}{n} \quad (11)$$

$$SI = \frac{RMSE}{y'} \quad (12)$$

$$OBJ = \left(\frac{n_{tr}}{n_{all}} * \frac{RMSE_{tr} + MAE_{tr}}{R_{tr}^2 + 1} \right) + \left(\frac{n_{tst}}{n_{all}} * \frac{RMSE_{tst} + MAE_{tst}}{R_{tst}^2 + 1} \right) + \left(\frac{n_{val}}{n_{all}} * \frac{RMSE_{val} + MAE_{val}}{R_{val}^2 + 1} \right) \quad (13)$$

where:

x_p and y_p are estimated and tested CS values; y' and x' are averages of experimentally tested and the estimated values from the models, respectively. *tr*, *tst*, and *val* referred to the training, testing, and validating datasets, respectively, and n is the number of datasets. Except for the R^2 value, 0 is the optimal value for all other evaluation parameters. However, 1 is the highest benefit for R^2. When it comes to the SI parameter, a model has bad performance when it is > 0.3, acceptable performance when it is 0.2 SI 0.3, excellent performance when it is 0.1 SI 0.2, and great performance when

it is 0.1 SI 0.1 (Faraj et al., 2021). Furthermore, the OBJ parameter was employed as a performance measurement parameter in Eq. (13) to measure the efficiency of the suggested models.

Results and analysis

(a) LR model

The output of this model revealed that the *l/b*, SS/SH, and *M* are those parameters that have a greater impact on the CS of GPC incorporated with nS than other parameters. This result was confirmed by a wide range of published experimental works in the literature (Hardjito et al. 2004; Deb et al. 2014; Oyebisi et al. 2020). Equation (14) with the weight of each model parameter is the output of this model. Optimizing the sum of error squares and the least square method, which were implemented in an Excel program using Solver to calculate the ideal value for the equation in one cell designated the objective cell, were used to determine the weighting of each parameter on the CS of GPC mixtures incorporating nS. The values of other equation cells constrained this object cell in the worksheet (Faraj et al., 2021).

$$\begin{aligned} CS = &110.06 - 66.6\left(\frac{l}{b}\right) + 0.06(b) - 0.01(FA) \\ &+ 0.005(CA) - 0.34(SH) + 0.12(SS) \\ &- 3.12(M) - 13.9\left(\frac{SS}{SH}\right) - 0.18(nS) + 0.11(T) \\ &+ 0.23(A) \end{aligned} \quad (14)$$

Figure 13a, b, and c depict the relationship between estimated and real CS of GPC mixtures incorporated with nS for training, testing, and validating datasets, respectively. Moreover, this model was evaluated by some statistical assessment tools, and it was observed that the R^2 and RMSE for the training datasets were equal to 0.7989 and 7.65 MPa, respectively, and as illustrated in Figs. 25 and 26, the other statistical criteria like OBJ and SI were 8.05 MPa and 0.209. Finally, utilizing training, testing, and validating datasets, the residual CS for the LR model for the forecasted and observed CS is displayed in Fig. 14.

(b) NLR model

The correlations between the actual and forecasted CS of GPC mixtures incorporated with nS are presented in Fig. 15a, b, and c for the training, testing, and validating datasets, correspondingly. As shown in Eq. (15), the weight of the model parameters demonstrated that the *l/b*, SH, and

Fig. 17 Comparison between tested and predicted CS of GPC mixtures incorporated with nS using MLR model: **a** training data, **b** testing data, **c** validating data
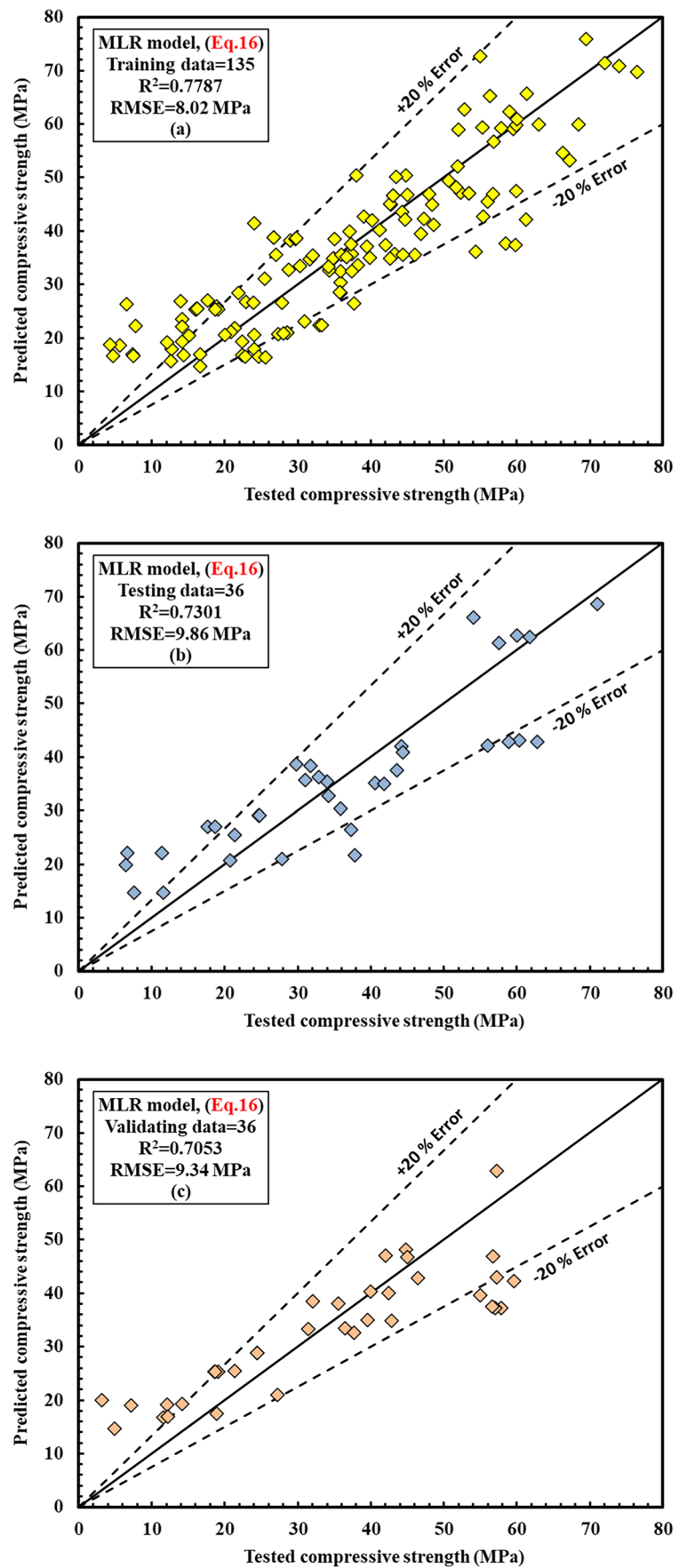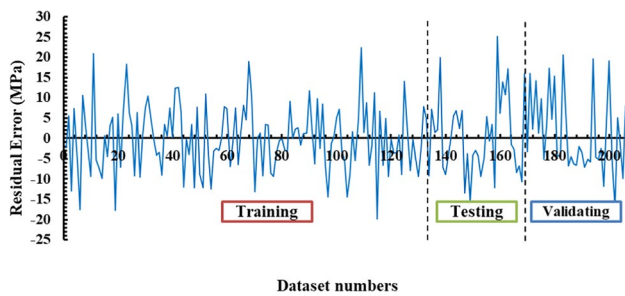
Fig. 18 Residual error diagram of CS of GPC mixtures incorporated with nS using training, testing, and validating datasets for MLR model

M are those input variable parameters that significantly affect the CS of geopolymer concrete mixtures modified with nS. This result was also well-validated in the previous experimental laboratory research works (Hardjito et al. 2004; Aliabdo et al. 2016; Ghafoor et al. 2021).

$$CS = -4643005 * \left(\frac{l}{b}\right)^{3.78} * (b)^{1.34} * (FA)^{-1.87}$$
$$* (CA)^{0.08} * (SH)^{5.5} * (SS)^{-7.85} * (M)^{2.72}$$
$$* \left(\frac{SS}{SH}\right)^{-6.06} * (T)^{-0.53} * (A)^{0.02} + 73.89$$
$$* \left(\frac{l}{b}\right)^{0.37} * (b)^{-0.03} * (FA)^{-0.45} * (CA)^{0.44} * (SH)^{-0.15} * (SS)^{-0.001}$$
$$* (M)^{-0.02} * \left(\frac{SS}{SH}\right)^{-0.15} * (T)^{0.0002} * (A)^{0.15} * (nS)^{0.002} \quad (15)$$

Similar to the LR model, this model was also assessed by some statistical criteria, and it was found that the R^2, RMSE, OBJ, and SI of the training datasets were equal to 0.8792, 5.92 MPa, 5.80 MPa, and 0.162, respectively. Furthermore,

the difference between actual and estimated CS of geopolymer concrete mixtures modified with nS can be found in Fig. 16 for all the validating, testing, and training datasets.

(iii) **MLR model**

Equation (16) shows the generated models for the MLR model with various variable parameters. The most significant independent factors that impact the CS of the geopolymer concrete mixtures modified with nS in the MLR model were SS content, age of the specimens, and curing temperatures, which are matched with some experimental studies published in the past articles (Jindal et al. 2017; Hassan et al. 2019; Ghafoor et al. 2021).

$$CS = 29.0347208 * \left(\frac{l}{b}\right)^{-1.47} * (b)^{0.04} * (FA)^{-0.21} * (CA)^{-0.26} * (SH)^{-0.09}$$
$$* (SS)^{0.56} * (M)^{-0.49} * \left(\frac{SS}{SH}\right)^{-0.22} * (nS)^{-0.005} * (T)^{0.13} * (A)^{0.2} \quad (16)$$

Figure 17a was created by utilizing training datasets to depict the anticipated and measured CS correlations for the GPC mixtures incorporated with nS. Furthermore, similar to the earlier models, this model was tested using two parts of data (validating and testing data) to demonstrate its efficacy for variables not included in the model data (training data). The findings indicate that by substituting the independent variables into the established equation, this model can predict the CS of GPC, as illustrated in Fig. 17b and c. The values of R^2 and RMSE for this developed model are 0.7787 and 8.02 MPa, respectively, for the training datasets. Also, as depicted in Figs. 25 and 26, the value of other statistical assessment tools like OBJ

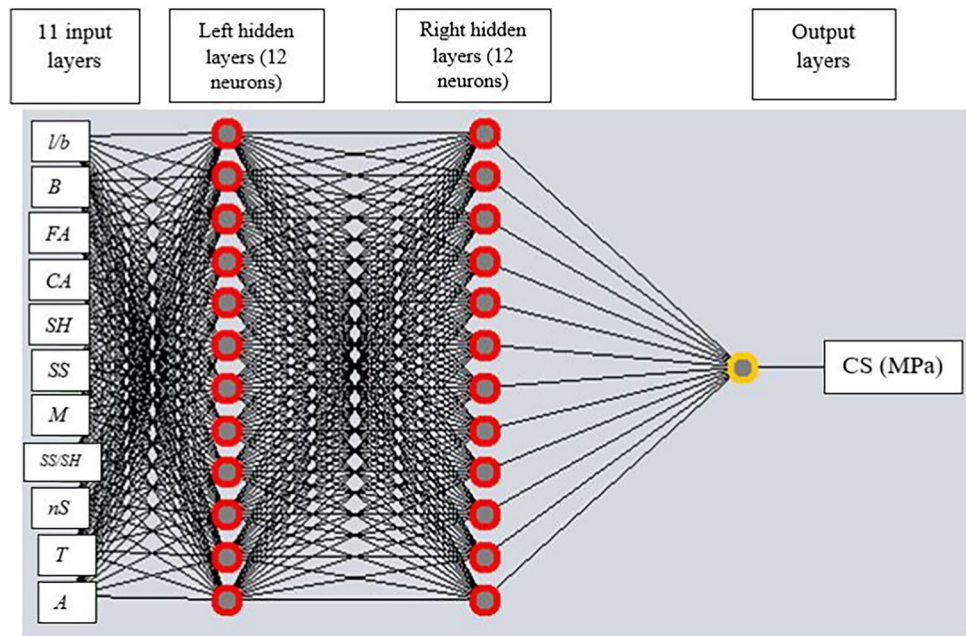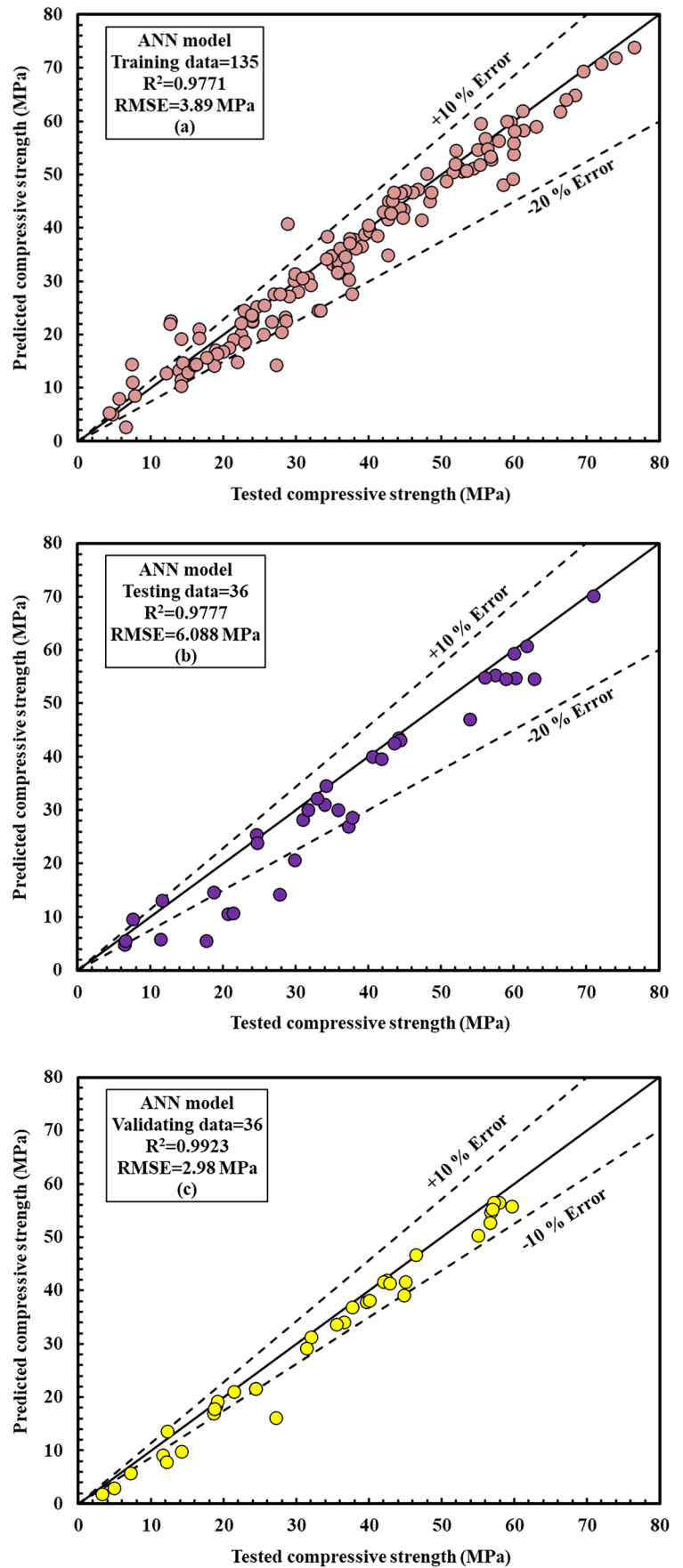**Fig. 19** Optimal network structures of the ANN model

Fig. 20 Comparison between tested and predicted CS of GPC mixtures incorporated with nS using ANN model: **a** training data, **b** testing data, **c** validating data
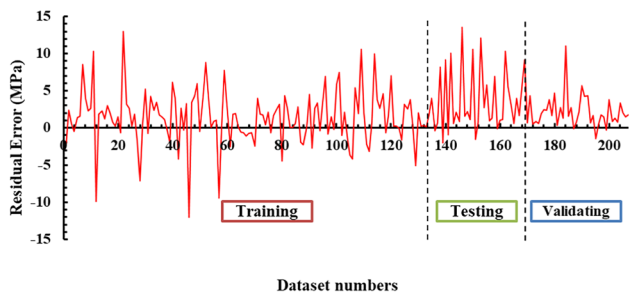
Fig. 21 Residual error diagram of CS of GPC mixtures incorporated with nS using training, testing, and validating datasets for ANN model

and SI values was observed at 8.8 MPa and 0.22, respectively. Lastly, utilizing validating, training, and testing data, the residual CS for the MLR model for predicted and observed CS of GPC incorporated with nS is displayed in Fig. 18.

(iv) **ANN model**

In this study, the authors tried a lot to get the high efficiency of the ANN by applying different numbers of the hidden layer, neurons, momentum, learning rate, and iteration, as can be seen in Table 3. Lastly, it was observed that when the ANN has two hidden layers, 24 neurons (12 for left side and 12 for the right side as shown in Fig. 19), 0.2 momenta, 0.1 learning rate, and 2000 iterations give the best-predicted values of the CS of the GPC mixtures incorporated with nS. The ANN model was equipped with the training datasets, accompanied by testing and validating datasets to predict the compression strength values for the correct input parameters. The comparisons between estimated and experimentally tested CS of GPC mixtures incorporated with nS for training, testing, and validating datasets are presented in Fig. 20a, b, and c. The consumed data have $+10\%$ and -20% error lines for the training and testing datasets, and $\pm10\%$ for the validating datasets, which is better than the other developed models. Furthermore, this model has a better performance than other models to predict the CS of the GPC incorporated with nS based on the value of OBJ and SI illustrated in Figs. 25 and 26. Also, the value of $R^2 = 0.9771$, MAE = 2.83 MPa, and RMSE = 3.89 MPa. Finally, the differences in the value of the CS for estimated and tested GPC mixtures incorporated with nS can be found in Fig. 21 by consuming all the datasets.

(e) **M5P model**

The predicted and observed CS of the GPC mixtures incorporated with nS for whole the datasets are shown in Fig. 22a, b, and c. Similar to the other models, it was discovered that the l/b and M of the GPC mixtures incorporated with nS have the greatest impact on the CS of the GPC mixtures incorporated with nS, which agrees with experimental findings in the past studies (Hardjito et al. 2004; Aliabdo et al. 2016; Ghafoor et al. 2021). Figure 23 shows the tree-shaped branch correlations. Also, the model (in Eq. (17)) parameters are summarized in Table 4, and the model variables will be selected based on the linear tree registration function.

$$
\begin{aligned}
CS = a + b\left(\frac{l}{b}\right) + c(b) + d(FA) + e(CA) \\
+ f(SH) + g(SS) + h(M) \\
+ i\left(\frac{SS}{SH}\right) + j(nS) + k(T) + l(A)
\end{aligned} \tag{17}
$$

For all of the training, testing, and validation datasets, there is a 20% error line. Finally, for all datasets, the residual CS for the M5P model was displayed in Fig. 24 for both predicted and observed CS. Furthermore, this model's R^2, RMSE, MAE, OBJ, and SI evaluation criteria are 0.9454, 5.59 MPa, 4.45 MPa, 6.0 MPa, and 0.153, respectively, for the training datasets.

Proposed models' performance

As early mentioned, the efficiency of the developed models was evaluated by employing these five stats tools: RMSE, MAE, SI, OBJ, and R^2. When compared to the LR, NLR, MLR, and M5P models, the ANN model has a higher R^2 with lower RMSE and MAE values, as well as lower OBJ and SI values.

In addition, Fig. 27 shows a comparison of model predictions of the CS of GPC mixtures incorporated with nS based on the testing datasets. Furthermore, Figs. 14, 16, 18, 21, and 24 display the residual errors for the CS by consuming all the datasets. The whole figures show that the estimated and tested CS values for the ANN model are close, indicating that the ANN model is more accurate than other models.

Figure 25 shows the OBJ values for all of the proposed models. The OBJ is 8.05, 5.8, 8.8, 3.59, and 6.0 for LR, NLR, MLR, ANN, and M5P, respectively. The ANN model has a lower OBJ value, about 124% less than the LR model, 61.5% less than the NLR model, 145% less than the MLR

Fig. 22 Comparison between tested and predicted CS of GPC mixtures incorporated with nS using M5P-tree model: **a** training data, **b** testing data, **c** validating data
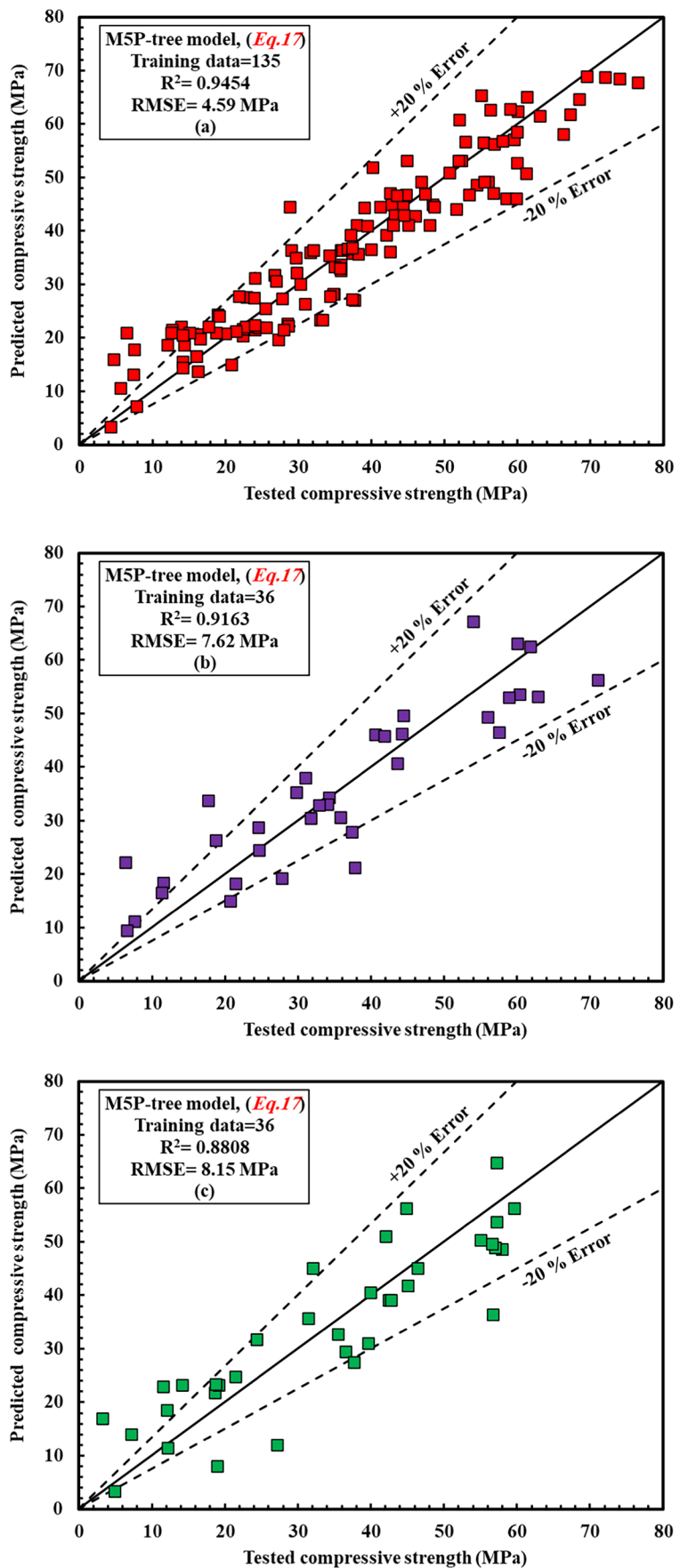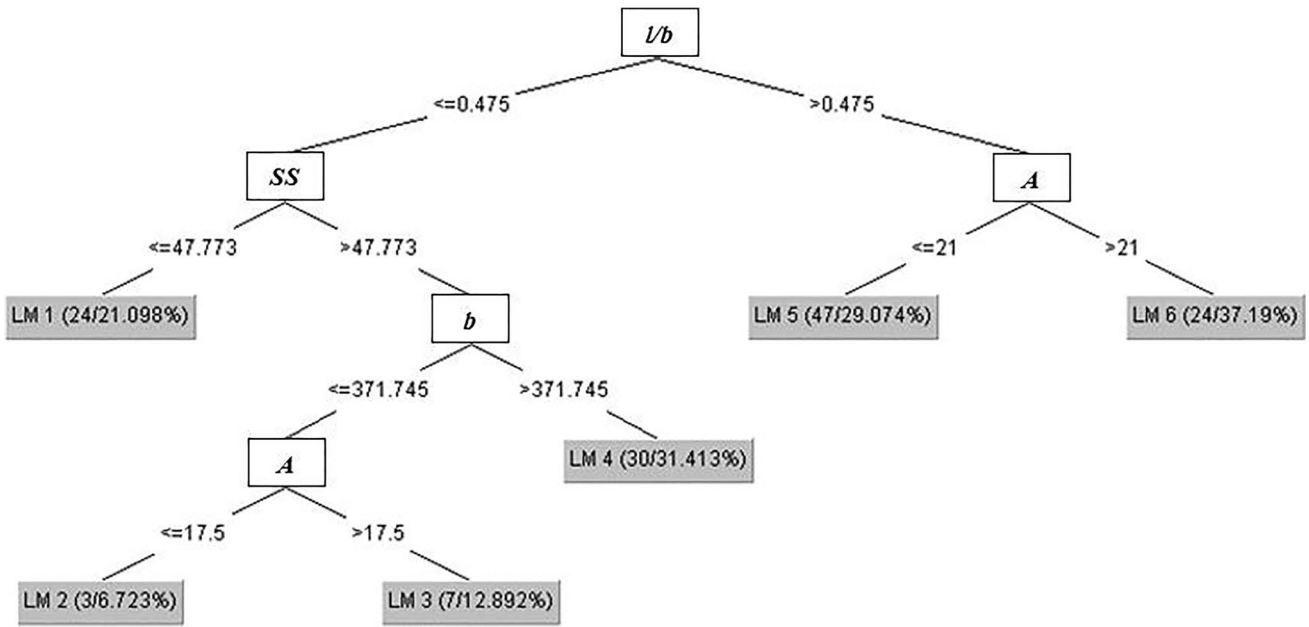
Fig. 23 M5P-tree pruned model tree

Table 4 M5P-tree model parameters (Eq. (17))

| (LM) num:	1	2	3	4	5	6
a	− 93.696	+ 32.7126	+ 32.8862	− 2.7578	− 166.0773	− 13.196
b	274.4776	38.4951	38.4951	38.4951	141.2642	53.0334
c	+ 0.0488	− 0.0138	− 0.0138	+ 0.0534	+ 0.1562	+ 0.0806
d					+ 0.0655	+ 0.024
e	+ 0.0029	+ 0.0077	+ 0.0077	+ 0.0174		− 0.0269
f	+ 0.2796	− 0.0513	− 0.0513	− 0.1534	− 0.0386	− 0.0386
g	− 0.0501	+ 0.0119	+ 0.0119	− 0.0114	− 0.0154	− 0.0154
h	− 0.5772	− 0.8632	− 0.8632	− 0.8632	− 0.4692	− 0.4692
i						
j	− 0.0307	− 0.0307	+ 0.0683	+ 0.0516	− 0.0282	− 0.0282
k					+ 0.3218	+ 0.077
l	+ 0.1921	+ 0.1625	+ 0.1575	+ 0.2233	+ 0.9407	+ 0.181
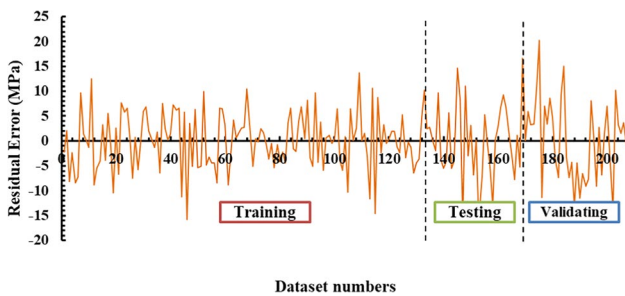
Fig. 24 Residual error diagram of CS of GPC mixtures incorporated with nS using training, testing, and validating datasets for M5P model
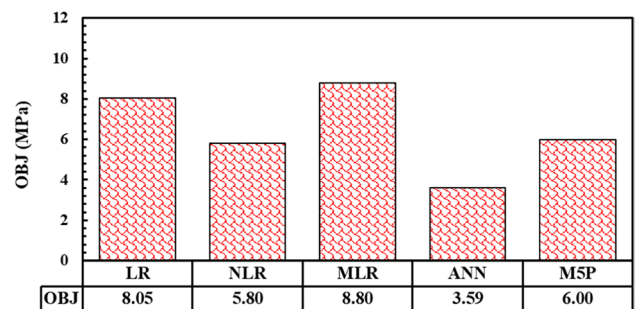

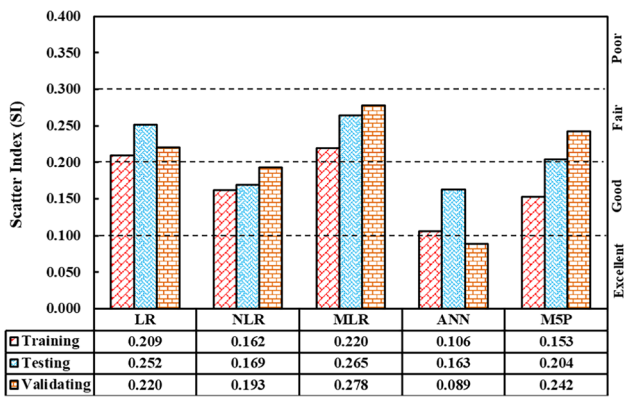**Fig. 25** The OBJ values of all developed models

Fig. 26 Comparing the SI performance parameters of different developed models
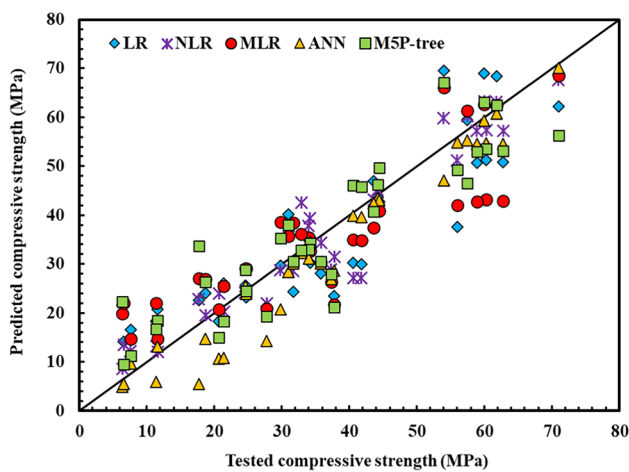

Fig. 27 Compression between model predictions of CS of GPC mixtures incorporated with nS using testing datasets

model, and 67% less than the M5P model. This also emphasized that the ANN model better forecasts the CS of GPC incorporated with nS.

In addition, Fig. 26 shows the SI values for the created models during the training, validating, and testing phases. The SI values for NLR and ANN models for the entire training, testing, and validating datasets were between 0.1 and 0.2, signalizing good accuracy for these models. While, for the other remaining models, the values of SI were between 0.2 and 0.3, this result revealed that the performance of the LR, MLR, and M5P models is in fair condition. Similar to other statistical assessment criteria, the ANN model has smaller SI values among the entire models. The ANN model has lower SI values (for training datasets) than the LR, NLR, MLR, and M5P models by 97.2%, 52.8%, 107.5%, and 44.3%, respectively. This also demonstrated that when forecasting the CS of GPC mixtures incorporated with nS,

the ANN model is more efficient and performs better than the other models (Fig. 27).

Conclusions

Using new scientifical technics like empirical correlations and neural networks to estimate the CS of GPC mixtures incorporated with nS can save time and money. LR, NLR, MLR, ANN, and M5P models were used in this article to develop predictive models for estimating the CS of GPC mixtures incorporated with nS. Based on the extensive revision and data gathering, the following conclusion can be drawn:

(i) The average amount of nS used in GPC mixtures was 11.6 kg/m^3, or approximately 3% of the binder content. Additionally, the percentage of nS substituted with binder varied between 0 and 60 kg/m^3.

(ii) The LR, NLR, MLR, ANN, and M5P models were all successfully utilized to create predictive models for the CS of the GPC mixtures incorporated with nS. The estimated CS closely matched experimentally measured CS of GPC mixtures that contained nS.

(iii) The whole created models satisfied all the statistical assessment criteria such as R^2, RMSE, MAE, OBJ, and SI.

(iv) The ANN model outperforms the other three models based on statistical evaluation and sensitivity analysis. For the training, testing, and validating datasets, the R^2 values are 0.9771, 0.9777, and 0.9923, respectively. Furthermore, the RMSE, MAE, OBJ, and SI stats criteria for the training dataset for the ANN model are 3.892 MPa, 2.832 MPa, 3.59 MPa, and 0.106, respectively. Consequently, the ANN model has greater generality and suitability in the initiatory design of GPC mixtures incorporated with nS.

(v) The two-layer ANN model with twelve neurons in each layer is the best model combination for estimating the CS of GPC mixtures incorporated with nS.

(vi) The sequence for suitability and having greater performances of the proposed models is as follows: ANN, NLR, M5P, LR, and MLR.

(vii) The obtained results indicate that the most significant variable parameters for estimating the CS of GPC mixtures which contained nS are the *l/b*, SS/SH, *M*, *T*, and *A*.

curation; writing—original draft; writing—review and editing for this manuscript.

Ahmed S. Mohammed: planning, validation; resources; data curation; writing—review for this manuscript.

Azad A. Mohammed: planning and designing; validation; writing—review for this manuscript.

Data availability Not applicable.

Declarations

Ethical approval Not applicable.

Consent to participate Not applicable.

Consent to publication Not applicable.

Competing interests The authors declare no competing interests.

References

Abdel-Gawwad HA, Abo-El-Enein SA (2016) A novel method to produce dry geopolymer cement powder. HBRC Journal 12(1):13–24. https://doi.org/10.1016/j.hbrcj.2014.06.008

Abdullah WA, Ahmed HU, Alshkane YM, Rahman DB, Ali AO, Abubakr SS (2021) The possibility of using waste PET plastic strip to enhance the flexural capacity of concrete beams. J Eng Res 9. https://doi.org/10.36909/jer.v9iICRIE.11649

Adak D, Sarkar M, Mandal S (2017) Structural performance of nano-silica modified fly-ash based geopolymer concrete. Constr Build Mater 135:430–439. https://doi.org/10.1016/j.conbuildmat.2016.12.111

Ahmed HU, Mohammed AA, Rafiq S, Mohammed AS, Mosavi A, Sor NH, Qaidi S (2021b) Compressive strength of sustainable geopolymer concrete composites: a state-of-the-art review. Sustainability 13(24):13502. https://doi.org/10.3390/su132413502

Ahmed HU, Mohammed AS, Mohammed AA, Faraj RH (2021c) Systematic multiscale models to predict the compressive strength of fly ash-based geopolymer concrete at various mixture proportions and curing regimes. PLoS ONE 16(6):e0253006. https://doi.org/10.1371/journal.pone.0253006

Ahmed HU, Faraj RH, Hilal N, Mohammed AA, Sherwani AFH (2021a) Use of recycled fibers in concrete composites: a systematic comprehensive review. Compos B Eng 108769. https://doi.org/10.1016/j.compositesb.2021a.108769

Ahmed HU, Mohammed AA, Mohammad AS (2022) The role of nanomaterials in geopolymer concrete composites: a state-of-the-art review. J Build Eng 104062. https://doi.org/10.1016/j.jobe.2022.104062

Aliabdo AA, Abd Elmoaty M, Salem HA (2016) Effect of water addition, plasticizer and alkaline solution constitution on fly ash based geopolymer concrete performance. Constr Build Mater 121:694–703. https://doi.org/10.1016/j.conbuildmat.2016.06.062

Angelin Lincy G, Velkennedy R (2020) Experimental optimization of metakaolin and nanosilica composite for geopolymer concrete paver blocks. Struct Concr. https://doi.org/10.1002/suco.201900555

Assaedi H, Shaikh FUA, Low IM (2016) Influence of mixing methods of nano silica on the microstructural and mechanical properties of flax fabric reinforced geopolymer composites. Constr Build Mater 123:541–552. https://doi.org/10.1016/j.conbuildmat.2016.07.049

Behfarnia K, Rostami M (2017) Effects of micro and nanoparticles of SiO2 on the permeability of alkali activated slag concrete. Constr Build Mater 131:205–213. https://doi.org/10.1016/j.conbuildmat.2016.11.070

Çevik A, Alzeebaree R, Humur G, Niş A, Gülşan ME (2018) Effect of nano-silica on the chemical durability and mechanical performance of fly ash based geopolymer concrete. Ceram Int 44(11):12253–12264. https://doi.org/10.1016/j.ceramint.2018.04.009

Davidovits J (2015) Geopolymer chemistry and applications. 4-th edition. J. Davidovits.–Saint-Quentin, France

Deb PS, Nath P, Sarker PK (2014) The effects of ground granulated blast-furnace slag blending with fly ash and activator content on the workability and strength properties of geopolymer concrete cured at ambient temperature. Mater Des 1980–2015(62):32–39. https://doi.org/10.1016/j.matdes.2014.05.001

Demircan E, Harendra S, Vipulanandan C (2011) Artificial neural network and nonlinear models for gelling time and maximum curing temperature rise in polymer grouts. J Mater Civ Eng 23(4):372–377. https://doi.org/10.1061/(ASCE)MT.1943-5533.0000172

Emad H, Soufi W, Elmannaey A, Abd-El-Aziz M, Hany EG (2018) Effect of nano-silica on the mechanical properties of slag geopolymer concrete

Etemadi M, Pouraghajan M, Gharavi H (2020) Investigating the effect of rubber powder and nano silica on the durability and strength characteristics of geopolymeric concretes. Journal of civil Engineering and Materials Application 4(4):243–252. https://doi.org/10.22034/jcema.2020.119979

Faraj RH, Mohammed AA, Mohammed A, Omer KM, Ahmed HU (2021) Systematic multiscale models to predict the compressive strength of self-compacting concretes modified with nanosilica at different curing ages. Eng Comput 1-24. https://doi.org/10.1007/s00366-021-01385-9

Faraj RH, Ahmed HU, Sherwani AFH (2022) Fresh and mechanical properties of concrete made with recycled plastic aggregates. In Handbook of sustainable concrete and industrial waste management (pp. 167–185). Woodhead Publishing. https://doi.org/10.1016/B978-0-12-821730-6.00023-1

Ghafoor MT, Khan QS, Qazi AU, Sheikh MN, Hadi MNS (2021) Influence of alkaline activators on the mechanical properties of fly ash based geopolymer concrete cured at ambient temperature. Constr Build Mater 273:121752. https://doi.org/10.1016/j.conbuildmat.2020.121752

Gholampour A, Mansouri I, Kisi O, Ozbakkaloglu T (2020) Evaluation of mechanical properties of concretes containing coarse recycled concrete aggregates using multivariate adaptive regression splines (MARS), M5 model tree (M5Tree), and least squares support vector regression (LSSVR) models. Neural Comput Appl 32(1):295–308. https://doi.org/10.1007/s00521-018-3630-y

Golafshani EM, Behnood A (2018) Application of soft computing methods for predicting the elastic modulus of recycled aggregate concrete. J Clean Prod 176:1163–1176. https://doi.org/10.1016/j.jclepro.2017.11.186

Golafshani EM, Behnood A, Arashpour M (2020) Predicting the compressive strength of normal and high-performance concretes using ANN and ANFIS hybridized with grey wolf optimizer. Constr Build Mater 232:117266. https://doi.org/10.1016/j.conbuildmat.2019.117266

Hamah Sor N, Hilal N, Faraj RH, Ahmed HU, Sherwani AFH (2021) Experimental and empirical evaluation of strength for sustainable lightweight self-compacting concrete by recycling high volume of industrial waste materials. European Journal of Environmental and Civil Engineering 1-18. https://doi.org/10.1080/19648189.2021.1997827

Hardjito D, Wallah SE, Sumajouw DM, Rangan BV (2004) On the development of fly ash-based geopolymer concrete. Materials Journal 101(6):467–472

Hassan A, Arif M, Shariq M (2019) Effect of curing condition on the mechanical properties of fly ash-based geopolymer concrete. SN Applied Sciences 1(12):1–9. https://doi.org/10.1007/s42452-019-1774-8

Ibrahim M, Johari MAM, Maslehuddin M, Rahman MK (2018a) Influence of nano-SiO2 on the strength and microstructure of natural pozzolan based alkali activated concrete. Constr Build Mater 173:573–585. https://doi.org/10.1016/j.conbuildmat.2018.04.051

Ibrahim M, Johari MAM, Rahman MK, Maslehuddin M, Mohamed HD (2018b) Enhancing the engineering properties and microstructure of room temperature cured alkali activated natural pozzolan based concrete utilizing nanosilica. Constr Build Mater 189:352–365. https://doi.org/10.1016/j.conbuildmat.2018.08.166

Ibrahim M, Rahman MK, Johari MAM, Maslehuddin M (2018c) Effect of incorporating nano-silica on the strength of natural pozzolan-based alkali-activated concrete. In International Congress on Polymers in Concrete (pp. 703–709). Springer, Cham. https://doi.org/10.1007/978-3-319-78175-4_90

Janaki AM, Shafabakhsh G, Hassani A (2021) Laboratory evaluation of alkali-activated slag concrete pavement containing silica fume and carbon nanotubes. Eng J 25(5):21–31. https://doi.org/10.4186/ej.2021.25.5.21

Jindal BB, Parveen, Singhal D, Goyal A (2017) Predicting relationship between mechanical properties of low calcium fly ash-based geopolymer concrete. Trans Indian Ceram Soc 76(4):258–265. https://doi.org/10.1080/0371750X.2017.1412837

Kotop MA, El-Feky MS, Alharbi YR, Abadel AA, Binyahya AS (2021) Engineering properties of geopolymer concrete incorporating hybrid nanomaterials. Ain Shams Eng J.https://doi.org/10.1016/j.asej.2021.04.022

Lazaro A, Yu QL, Brouwers HJH (2016) Nanotechnologies for sustainable construction. In Sustainability of construction materials (pp. 55–78). Woodhead Publishing

Mahasenan N, Smith S, Humphreys K (2003) The cement industry and global climate change: current and potential future cement industry CO2 emissions. In Greenhouse Gas Control Technologies-6th International Conference (pp. 995–1000). Pergamon

Mahboubi B, Guo Z, Wu H (2019) Evaluation of durability behavior of geopolymer concrete containing nano-silica and nano-clay additives in acidic media. Journal of civil Engineering and Materials Application 3(3):163–171. https://doi.org/10.22034/JCEMA.2019.95839

Malerba D, Esposito F, Ceci M, Appice A (2004) Top-down induction of model trees with regression and splitting nodes. IEEE Trans Pattern Anal Mach Intell 26(5):612–625. https://doi.org/10.1109/TPAMI.2004.1273937

Mohammed AS (2018) Vipulanandan models to predict the electrical resistivity, rheological properties and compressive stress-strain behavior of oil well cement modified with silica nanoparticles. Egypt J Pet 27(4):1265–1273. https://doi.org/10.1016/j.ejpe.2018.07.001

Mohammed AA, Ahmed HU, Mosavi A (2021) Survey of mechanical properties of geopolymer concrete: a comprehensive review and data analysis. Materials 14(16):4690. https://doi.org/10.3390/ma14164690

Mustakim SM, Das SK, Mishra J, Aftab A, Alomayri TS, Assaedi HS, Kaze CR (2020) Improvement in fresh, mechanical and microstructural properties of fly ash-blast furnace slag based geopolymer concrete by addition of nano and micro silica. Silicon 1-14. https://doi.org/10.1007/s12633-020-00593-0

Naskar S, Chakraborty AK (2016) Effect of nano materials in geopolymer concrete. Perspect Sci 8:273–275. https://doi.org/10.1016/j.pisc.2016.04.049

Nuaklong P, Sata V, Wongsa A, Srinavin K, Chindaprasirt P (2018) Recycled aggregate high calcium fly ash geopolymer concrete with inclusion of OPC and nano-SiO2. Constr Build Mater 174:244–252. https://doi.org/10.1016/j.conbuildmat.2018.04.123

Nuaklong P, Jongvivatsakul P, Pothisiri T, Sata V, Chindaprasirt P (2020) Influence of rice husk ash on mechanical properties and fire resistance of recycled aggregate high-calcium fly ash geopolymer concrete. J Clean Prod 252:119797. https://doi.org/10.1016/j.jclepro.2019.119797

Oyebisi S, Ede A, Olutoge F, Omole D (2020) Geopolymer concrete incorporating agro-industrial wastes: effects on mechanical properties, microstructural behaviour and mineralogical phases. Constr Build Mater 256:119390. https://doi.org/10.1016/j.conbuildmat.2020.119390

Patel Y, Patel IN, Shah MJ (2015) Experimental investigation on compressive strength and durability properties of geopolymer concrete incorporating with nano silica. International Journal of Civil Engineering and Technology 6(5):135–143

Provis JL, Palomo A, Shi C (2015) Advances in understanding alkali-activated materials. Cem Concr Res 78:110–125. https://doi.org/10.1016/j.cemconres.2015.04.013

Qaidi SM, Tayeh BA, Zeyad AM, de Azevedo AR, Ahmed HU, Emad W (2022) Recycling of mine tailings for the geopolymers production: a systematic review. Case Studies in Construction Materials e00933. https://doi.org/10.1016/j.cscm.2022.e00933

Quinlan Ross J (1992) Learning with continuous classes. In: 5th Australian Joint Conference on Artificial Intelligence, Singapore, pp. 343–348

Rabiaa E, Mohamed RAS, Sofi WH, Tawfik TA (2020) Developing geopolymer concrete properties by using nanomaterials and steel fibers. Adv Mater Sci Eng 2020. https://doi.org/10.1155/2020/5186091

Ravitheja A, Kumar NK (2019) A study on the effect of nano clay and GGBS on the strength properties of fly ash based geopolymers. Materials Today: Proceedings 19:273–276. https://doi.org/10.1016/j.matpr.2019.06.761

Roco MC, Williams RS, Alivisatos P (Eds.) (2000) Nanotechnology research directions: IWGN workshop report: vision for nanotechnology in the next decade. Springer Science & Business Media

Saini G, Vattipalli U (2020) Assessing properties of alkali activated GGBS based self-compacting geopolymer concrete using nano-silica. Case Studies in Construction Materials 12:e00352. https://doi.org/10.1016/j.cscm.2020.e00352

Sastry KGK, Sahitya P, Ravitheja A (2021) Influence of nano TiO2 on strength and durability properties of geopolymer concrete. Materials Today: Proceedings 45:1017–1025. https://doi.org/10.1016/j.matpr.2020.03.139

Shahmansouri AA, Yazdani M, Ghanbari S, Bengar HA, Jafari A, Ghatte HF (2020b) Artificial neural network model to predict the compressive strength of eco-friendly geopolymer concrete incorporating silica fume and natural zeolite. J Clean Prod 279:123697. https://doi.org/10.1016/j.jclepro.2020.123697

Shahmansouri AA, Bengar HA, Ghanbari S (2020a) Compressive strength prediction of eco-efficient GGBS-based geopolymer concrete using GEP method. J Build Eng 101326. https://doi.org/10.1016/j.jobe.2020a.101326

Shahrajabian F, Behfarnia K (2018) The effects of nano particles on freeze and thaw resistance of alkali-activated slag concrete. Constr Build Mater 176:172–178. https://doi.org/10.1016/j.conbuildmat.2018.05.033

Shaikh FUA (2016) Mechanical and durability properties of fly ash geopolymer concrete containing recycled coarse aggregates. Int J Sustain Built Environ 5(2):277–287. https://doi.org/10.1016/j.ijsbe.2016.05.009

Sharif HH (2021) Fresh and mechanical characteristics of eco-efficient geopolymer concrete incorporating nano-silica: an

overview. Kurdistan Journal of Applied Research, 64–74. https://doi.org/10.24017/science.2021.2.6

Sihag P, Jain P, Kumar M (2018) Modelling of impact of water quality on recharging rate of storm water filter system using various kernel function based regression. Modeling Earth Systems and Environment 4(1):61–68. https://doi.org/10.1007/s40808-017-0410-0

Their JM, Özakça M (2018) Developing geopolymer concrete by using cold-bonded fly ash aggregate, nano-silica, and steel fiber. Constr Build Mater 180:12–22. https://doi.org/10.1016/j.conbuildmat.2018.05.274

Velay-Lizancos M, Perez-Ordoñez JL, Martinez-Lage I, Vazquez-Burgo P (2017) Analytical and genetic programming model of compressive strength of eco concretes by NDT according to curing temperature. Constr Build Mater 144:195–206. https://doi.org/10.1016/j.conbuildmat.2017.03.123

Vyas, S., Mohammad, S., Pal, S., & Singh, N. (2020). Strength and durability performance of fly ash based geopolymer concrete using nano silica. *International Journal of Engineering Science Technologies*, *4*(2), 1–12. https://doi.org/10.29121/ijoest.v4.i2.2020.73

Weil M, Dombrowski K, Buchwald A (2009) Life-cycle analysis of geopolymer. In Geopolymers (pp. 194–210). Woodhead Publishing. https://doi.org/10.1533/9781845696382.2.194

Wiesner MR, Bottero JY (2017) Environmental nanotechnology: applications and impacts of nanomaterials. McGraw-Hill Education. https://www.accessengineeringlibrary.com/content/book/9780071828444

Yildirim G, Sahmaran M, Ahmed HU (2015) Influence of hydrated lime addition on the self-healing capability of high-volume fly ash incorporated cementitious composites. J Mater Civ Eng 27(6):04014187. https://doi.org/10.1061/(ASCE)MT.1943-5533.0001145

Publisher's note Springer Nature remains neutral with regard to jurisdictional claims in published maps and institutional affiliations.